



# VCU

Virginia Commonwealth University  
VCU Scholars Compass

---

Theses and Dissertations

Graduate School

---

2003

## AFM, CAFM, and EFM Studies of the GaN System

John C. Dickinson

Follow this and additional works at: <https://scholarscompass.vcu.edu/etd>



Part of the [Physics Commons](#)

© The Author

---

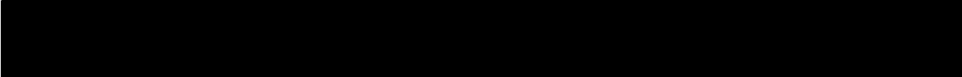
Downloaded from

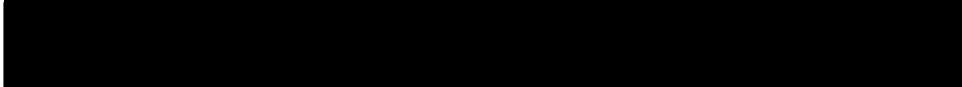
<https://scholarscompass.vcu.edu/etd/4522>

This Thesis is brought to you for free and open access by the Graduate School at VCU Scholars Compass. It has been accepted for inclusion in Theses and Dissertations by an authorized administrator of VCU Scholars Compass. For more information, please contact [libcompass@vcu.edu](mailto:libcompass@vcu.edu).

**College of Humanities and Sciences  
Virginia Commonwealth University**

This is to certify that the thesis prepared by John C. Dickinson entitled "AFM, CAFM, and EFM of the GaN System" has been approved by his committee as satisfactory completion of the thesis requirements for the degree of Master of Science.

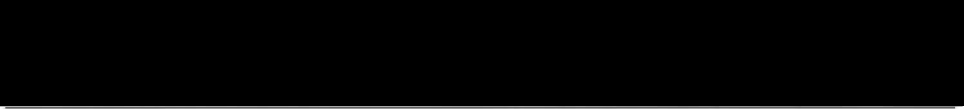
  
Dr. Alison Baski, College of Humanities and Sciences

  
Dr. David Ameen, College of Humanities and Sciences

  
Dr. Hadis Morkoç, School of Engineering

  
Dr. Robert Gowdy, Chairman of Physics

  
Dr. Stephen Gottfredson, Dean of the College of Humanities and Sciences

  
Dr. F. Douglas Boudinot, Dean of the School of Graduate Studies

April 23, 2003  
Date

# **AFM, CAFM, and EFM Studies of the GaN System**

A thesis submitted in partial fulfillment of the requirements for the degree of Master of Science in Physics / Applied Physics at Virginia Commonwealth University.

By

John Chalmers Dickinson

B.S. in Physics

Virginia Commonwealth University, 2000

M.S. in Physics/Applied Physics

Virginia Commonwealth University, 2003

Director: Alison. A. Baski, Associate Professor, Department of Physics

Virginia Commonwealth University,

Richmond, Virginia, 23284

April 23, 2003

## Acknowledgements

I would like to thank my parents Paul and Judy Dickinson; I can't even express how much ya'll mean to me. Jane, my sister, thanks for listening to the drama that seemingly sprouts up everywhere and helping me deal with it, may Nursing give you the gratification that you definitely deserve. My bro Paul and my sister-in-law Alison have helped me improve my life by listening to my incessant babbling and somehow figured out what I was saying to give me advice. Without all of their constant babbling on the phone, I would have no idea what goes on in the family. I'd like to thank my childhood dog Fuzzy and my dog Thea, who passed away this past year, for the memories of relaxation running around in the yard hunting whatever new scent you found. To my grandmother Jane Flinn I know I haven't been around that much to help you, but you taught me how to be an honorable man. To my grandmother Elsie Dickinson, I know I haven't been able to help you either, but thank you for teaching me how a southern gentleman should act. To all of my Physics professors, who had to put up with me, thanks for teaching me. I won't forget any of you. Dr. David Ameen, well I'm sorry that I made you read this, but thanks for helping me make something of my self. Dr. Hadis Morkoç, after watching you I know what it takes to be on the top, I could only wish to be that great. Dr. Alison Baski, well, I know I haven't been the best student that has gone through the undergrad and grad programs, but I know that what you taught me in the 6 years will help me with whatever career I go into and will help me teach any of those poor souls in the future. Thank you all, and goodbye.

This work was partially supported by the National Science Foundation.

## Table of Contents

Acknowledgements.....	ii
List of Figures .....	iv
Abstract .....	vi
Chapter 1. Atomic Force Microscopy (AFM) and Conductive AFM.....	1
1.1 Atomic Force Microscopy (AFM).....	1
1.2 Conductive Atomic Force Microscopy (CAFM).....	3
1.3 Chapter 1 Figures.....	6
Chapter 2. Surface Potential Electric Force Microscopy .....	23
2.1 Technique .....	23
2.2 Detection of Inversion Domains .....	24
2.3 Application to Modulation Doped Field Effect Transistors .....	25
2.4 Chapter 2 Figures.....	28
References .....	41

## List of Figures

Fig. 1.1: Schematic of AFM technique. ....	6
Fig. 1.2: (a) Si cantilever used primarily for tapping mode AFM and (b) Si <sub>3</sub> N <sub>4</sub> cantilever used for contact mode AFM. ....	7
Fig. 1.3: Tapping mode cantilever holder. ....	8
Fig. 1.4: (a) Dimension 3100 AFM unit and (b) schematic of AFM head. ....	9
Fig. 1.5: AFM Data Screen with important icons and data values highlighted. ....	10
Fig. 1.6: AFM images of Ga-polar GaN, where the z-height data range and image size are indicated in the lower right corner of each image. ....	11
Fig. 1.7: AFM images of N-polar GaN, which is significantly more rough than Ga-polar GaN (compare to Fig. 1.6). ....	12
Fig. 1.8: Conductive AFM (CAFM) and Tunneling AFM (TUNA) techniques, where a tip-sample current is measured for an applied DC bias voltage. ....	13
Fig. 1.9: (a) AFM head and CAFM module attachment, (b) close-up of module, and (c) CAFM cantilever holder with current detection. ....	14
Fig. 1.10: CAFM Data Screen with important values highlighted. ....	15
Fig. 1.11: TUNA Data Screen with important values highlighted. ....	16
Fig. 1.12: (a, b) AFM & CAFM and (c,d) AFM & TUNA images of etch pits on n-type GaN using positive sample bias (reverse-bias). ....	17
Fig. 1.13: Cross sections for CAFM and TUNA images shown in Fig. 1.12. ....	18
Fig. 1.14: (a, b) AFM & CAFM and (c,d) AFM & TUNA images of etch pits on n-type GaN with negative sample bias (forward-bias). ....	19
Fig. 1.15: Cross sections for CAFM and TUNA images shown in Fig. 1.14. ....	20
Fig. 1.16: (a, b) AFM & CAFM and (c,d) AFM & TUNA images of p-type GaN with positive sample bias (forward-bias). ....	21
Fig. 1.17: Cross sections for CAFM and TUNA images shown in Fig. 1.16. ....	22
Fig. 2.1: Step-by-step explanation of Surface Potential Electric Force Microscopy (SP-EFM) technique. ....	28

Fig. 2.2: Continuation of Fig. 2.1.....	29
Fig. 2.3: SP-EFM Data Screen with important values highlighted.....	30
Fig. 2.4: (a) Crystal structures for N-polar and Ga-polar GaN and (b) schematic of local surface charging caused by domains of opposite polarity.....	31
Fig. 2.5: (a) AFM and (b) SP-EFM images of an inversion domain on Ga-polar GaN grown with ammonia, where a cross section (c) indicates a voltage difference of 90 mV for the N-polar domain.....	32
Fig. 2.6: (a) AFM and (b) SP-EFM images of an inversion domain on Ga-polar GaN, where a cross section (c) indicates a voltage difference of 30 mV for the N-polar domain.....	33
Fig. 2.7: (a) AFM and (b) SP-EFM images of an inversion domain on Ga-polar GaN. Cross sections of SP-EFM data are shown for lift heights of (c) 80 nm and (d) 400 nm, where larger lift heights result in a larger voltage difference for the inversion domain.....	34
Fig. 2.8: (a) Schematic of a GaN/AlGaN Modulated Doped Field Effect Transistor (MODFET). (b) Band diagram showing the 2-dimensional electron gas (2DEG) that forms in the active GaN layer.....	35
Fig. 2.9: (a) Optical image of MODFET #1 with an AlGaN top layer. (b) AFM and (c) SP-EFM images taken without applied voltage. (d) Cross section of SP-EFM data indicating a 13 mV voltage difference between gate metallization and AlGaN top layer.....	36
Fig. 2.10: (a,c) AFM and (b,d) SP-EFM images of MODFET #1 with a <i>negative</i> applied gate voltage of $-0.55$ V with respect to the source. ....	37
Fig. 2.11: (a,c) AFM and (b,d) SP-EFM images of MODFET #1 with a <i>positive</i> applied gate voltage of $0.67$ V with respect to the drain.....	38
Fig. 2.12: (a,c) AFM and (b,d) SP-EFM images of MODFET #2 with a <i>negative</i> applied gate voltage of $-1.0$ V with respect to the source. ....	39
Fig. 2.13: (a,c) AFM and (b,d) SP-EFM images of MODFET #2 with a <i>negative</i> applied gate voltage of $-0.55$ V with respect to the source. ....	40

## **Abstract**

By John C. Dickinson, M.S.

A thesis submitted in partial fulfillment of the requirements for the degree of  
Master of Science at Virginia Commonwealth University, 2003.

Major Director: Alison A. Baski, Associate Professor, Department of Physics

This thesis discusses a variety of techniques based on the atomic force microscope (AFM), and their application to the GaN materials system. In particular, the local conductivity and contact potential of surfaces have been measured using the techniques of Conductive AFM (CAFM) and Surface Potential Electric Force Microscopy (SP-EFM), respectively. CAFM studies of GaN surfaces have revealed that prismatic planes around islands and pits on surfaces can lead to enhanced conductivity, which may be related to leakage problems in device applications. With regard to SP-EFM work, the change in surface potential associated with inversion domains on Ga-polar GaN has been imaged, yielding voltage differences up to 90 mV. Given that such inversion domains increase carrier scattering and can degrade device performance, their identification using this technique is important. SP-EFM has also been used to map the local surface potential in the active region of Modulation Doped Field Effect Transistors (MODFET's). This is the first step in a proposed study to investigate the effects of current lag in such devices.



## Chapter 1. Atomic Force Microscopy (AFM) and Conductive AFM

### 1.1 Atomic Force Microscopy (AFM)

The first Atomic Force Microscope (AFM) was developed in 1986 as the result of a collaboration between IBM (Binnig and Gerber) and Stanford University (Quate). After the invention of the scanning tunneling microscopy (STM) in 1982, the need was recognized for another microscopy technique that could examine insulating surfaces using a force mechanism. The original AFM prototype measured the deflections of a gold foil lever as it was scanned across a surface. Since those early days, commercial instruments have become available that integrate micromachined cantilevers with laser motion detection. Today, the AFM has become an important research tool for studying surfaces in disciplines ranging from materials science to biology.

In the basic AFM design, a micro-machined cantilever is brought into contact with a surface and the tip-sample force is monitored during scanning. The force measurement is done by reflecting a laser beam off the backside of the cantilever and monitoring its location with a photodetector (see Fig. 1.1). As the cantilever bends due to tip-sample forces, the laser beam moves on the detector. In contact mode AFM, the tip and sample are always in contact and a feedback circuit maintains a constant tip-sample force during scanning. The vertical height of the cantilever above the surface is adjusted in order to always maintain a constant cantilever deflection, or tip-sample force. This corresponds to maintaining a fixed position of the reflected laser beam on the photodetector. In another variation of AFM, known as Tapping Mode<sup>TM</sup> AFM, the cantilever is vibrated at its resonance frequency during scanning. The cantilever is then approached to the surface until it touches *only* during each “down” cycle of its oscillation. A feedback loop then controls the tip-sample force by keeping a constant oscillation amplitude during scanning. An advantage of tapping-mode AFM is the reduction of lateral forces that can damage the tip and/or surface.

The cantilevers used in AFM are typically micro-machined from Si or Si<sub>3</sub>N<sub>4</sub> in order to achieve the necessary low force constants (~1 N/m) and high resonant frequencies (50-500 kHz). To improve resolution, all cantilevers have an integrated tip with a diameter of

40–120 nm for  $\text{Si}_3\text{N}_4$  cantilevers and 10–20 nm for Si cantilevers. Figure 1.2 shows typical cantilevers used for tapping and contact mode AFM. Tapping mode cantilevers usually have larger force constants (20–100 N/m) and higher resonant frequencies (200–400 kHz) than those used for contact mode. The two most common geometries are a “diving board” constructed from Si, or a V-shape constructed from  $\text{Si}_3\text{N}_4$ . In our system, the cantilevers are mounted in a grooved holder such as the one pictured in Fig 1.3, and are held in place by a spring clip. Located under the groove is a piezoelectric stack that is used to oscillate the cantilever for tapping mode AFM.

A photograph of our Dimension 3100 AFM is shown in Fig. 1.4 [1]. A sample is placed on the chuck plate and can be moved on a translational stage using computer controls. Above the sample, the AFM head includes the laser, cantilever, piezoelectric tube scanner, and photodetector integrated into one unit. An optical microscope is mounted to the side of the head in order to locate the tip and sample with respect to each other. After the sample is mounted on the chuck, the laser beam is aligned on the cantilever by using two knobs located on top of the head, and aligned on the photodetector using two knobs located on the left. For tapping mode AFM, the cantilever must then be “tuned” to its resonant frequency using an automatic routine in the data program (click Tuning icon shown in Fig. 1.5). Note that sometimes an unusually large drive amplitude ( $> 1.4$  V) is necessary to oscillate the cantilever such that it produces a reasonable photodetector signal. This indicates that the cantilever may not be properly mounted on its holder, or that the holder needs cleaning. After the tuning procedure has been successfully completed, the tip and sample must be properly “located” in order to proceed with a computerized approach. The trackball control for the stage motion is used to move the relative positions of the tip and sample so that they are in focus using the optical microscope (click on Focus Sample or Focus Tip icons). Lastly, the cantilever must be approached to the sample in order to begin taking data (click Engage icon).

After the tip is engaged on the sample, the user must optimize parameters such as the tip-sample force and feedback gains. First, the scope trace should be examined to determine if the cantilever is properly following the sample morphology (click Scope Trace icon). The topographical trace (left to right) and retrace (right to left) should

appear nearly identical. If they are not, then the tip-sample force must be typically increased. Use the Amplitude (or Force) Setpoint value in the Feedback Controls menu to set the force (min. value of  $\sim 1$  V), where a *smaller* setpoint value actually corresponds to a *larger* force in Tapping Mode AFM. This is because the setpoint indicates the amplitude range of the vibrating cantilever. This value is largest when the cantilever is in “free” oscillation above the surface, and decreases as the tip is brought closer to the surface and experiences a greater force. Once the optimal force has been achieved, then the feedback gains must be adjusted. Common values for the integral and proportional gains are given in Fig 1.5. After these parameters have been optimized, then the AFM image can be displayed again (click Image Mode icon).

Figures 1.6 and 1.7 illustrate typical AFM morphologies observed for Ga-polar and N-polar MBE-grown GaN samples. The polarity indicates the crystal orientation in the  $c$ -axis growth direction (see Fig. 2.4). The Ga-polar sample in Fig. 1.6 is a  $1.2\ \mu\text{m}$ -thick film grown at  $\sim 800^\circ\text{C}$  on an AlN buffer layer, with ten alternating layers of AlN and GaN below the GaN to minimize defect propagation (sample #381) [2]. The images show a relatively smooth surface with a surface height rms value of  $\sim 3$  nm. A small density of hexagonal islands appear that have been shown to correspond to inversion domains on the surface, i.e. local N-polarity regions [3]. As shown in the higher resolution image of Fig. 1.6b, these islands are  $\sim 300$  nm in diameter and  $\sim 30$  nm tall. Note that the  $z$  height data range and image size are given in the lower right corner of each image. For comparison, a N-polar sample is shown in Fig. 1.7 (sample #618), which is significantly more rough (rms value  $\cong 20$  nm). This sample was grown at  $\sim 500^\circ\text{C}$  on an AlN buffer using a lower growth rate than for the Ga-polar sample [4]. The resulting morphology shows isolated islands with heights of 50 to 80 nm. These AFM images demonstrate that the distinctive morphologies of the N- and Ga-polar surfaces can be used as a preliminary method of crystal orientation identification.

## 1.2 Conductive Atomic Force Microscopy (CAFM)

In addition to topographical information, local conductivity data can be acquired using a variation of AFM known as Conductive AFM (CAFM) or Tunneling AFM

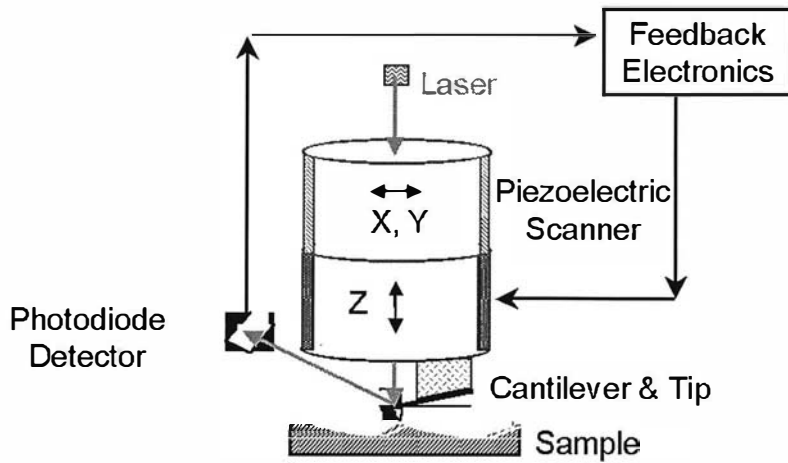
(TUNA) [5]. In this case, the AFM is operated in *contact* mode with an electrically conductive cantilever connected to an external voltage source (see Fig. 1.8). Both metal-coated or highly doped diamond-coated tips are used. The sample must also be electrically connected to this circuit, typically with silver paint in our experiments. During scanning, a DC bias voltage is applied to the sample and a low-noise amplifier detects the localized current between the tip and sample. CAFM (or TUNA) is performed by adding a specialized module to the AFM head and mounting the cantilever in a holder with a current output (see Fig. 1.9). The module contains a test connector for calibration and a sensor input connector for connection with the cantilever holder. During operation, the tip-sample force (deflection setpoint) and DC bias voltage are then adjusted to optimize contrast between low and high conductivity regions on the surface (see data screen in Fig. 1.10). Note that in the case of *contact* mode operation, the setpoint value is set *larger* for larger tip-sample forces, which is opposite the case for tapping mode operation.

Current measurements were taken of etched GaN samples using both CAFM and TUNA [6]. These samples were grown using hydride vapor-phase epitaxy (HVPE) on *c*-plane sapphire and then etched to reveal dislocation defects. Figures 1.12 to 1.15 show results for a Si-doped, *n-type* GaN sample ( $n \sim 2 \times 10^{18} \text{ cm}^{-3}$ , 9.4  $\mu\text{m}$  thick), where the sample was etched with KOH (6 min at 210 °C). The etching process preferentially removes material at dislocation defects, producing hexagonal etch pits at such locations [7]. CAFM and TUNA both show enhanced current at the edges of the pits for both reverse and forward-bias conditions. In reverse bias (i.e. positive sample bias), the current cross sections in Fig. 1.13 indicate maximum values between 50 to 100 pA for CAFM (or  $\sim 150 \text{ G}\Omega$ ), but only a “maximum” value of 10 pA for TUNA. This discrepancy is a consequence of the limited current range for the TUNA module. It should also be noted that in CAFM there are isolated regions on the sample which indicate currents up to the maximum value of 10 nA. Figs. 1.14 and 1.15 show the same sample under forward-bias conditions, where CAFM indicates a maximum current of  $\sim 10 \text{ nA}$  (or  $\sim 100 \text{ M}\Omega$ ). As expected, the measured current values are significantly higher for forward bias vs. reverse bias conditions.

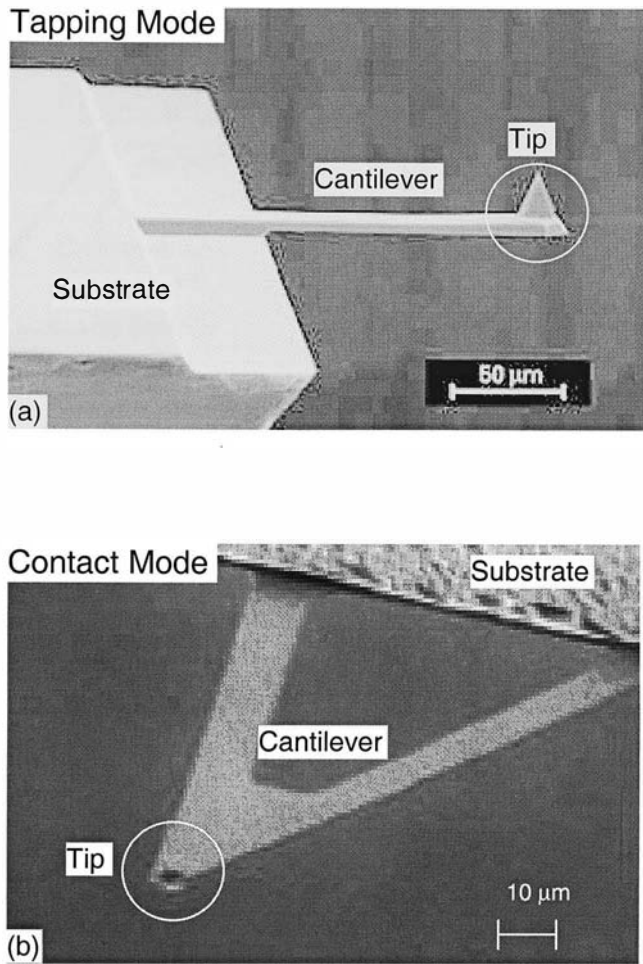
The behavior for nominally *p-type* GaN is similar to n-type, but no measurable current is found under reverse-bias conditions. The p-type sample shown in Fig. 1.16 is an HVPE sample doped with Zn and then etched with phosphoric acid at 160°C for 2 min. Under forward bias, both CAFM and TUNA indicate comparable currents (~40 and 30 pA) around the etch pits. This corresponds to a local resistivity of ~100 GΩ at the edges of the etch pits, a value that is significantly higher than observed for forward-bias conditions for n-type samples. This may be primarily due to the higher bulk resistivity of the Zn-doped sample as compared to the n-type one. In conclusion, our CAFM results indicate that the off-axis or “prismatic” planes at the edges of etch pits are more electrically active than c-plane GaN. This enhanced conduction could be related to their origin near defect sites.

It should be noted that prior CAFM studies have shown that dislocations may in fact provide channels for large and stable current. Investigations by Hsu et al. have shown that reverse bias current on Pt contacts on MBE-grown GaN samples is concentrated at dislocations with a screw component, which occurs at the tops of hillocks [8]. They observe that the growth process and stoichiometry affect the electrical activity and core structure of dislocations, where dislocations in films grown under Ga-rich conditions possess larger leakage current than those under Ga-lean conditions [9]. Miller et al. also observed conductive screw or mixed dislocations in MBE-grown GaN/AlGaIn heterostructures under reverse bias, although dislocations with a screw component that did not conduct current were also apparent in their study [10]. Our studies do not indicate any leakage current through dislocations *until* the sample has been etched, in which case pits are formed in the regions of dislocations. A study by Shiojima et al. is more consistent with our observations, where neither mixed nor pure edge dislocations were found to affect the IV characteristics for CAFM measurements of Schottky contacts on GaN [11]. On the other hand, they did find that large structural defects such as “nanopipes” could lead to large currents and short the contact.

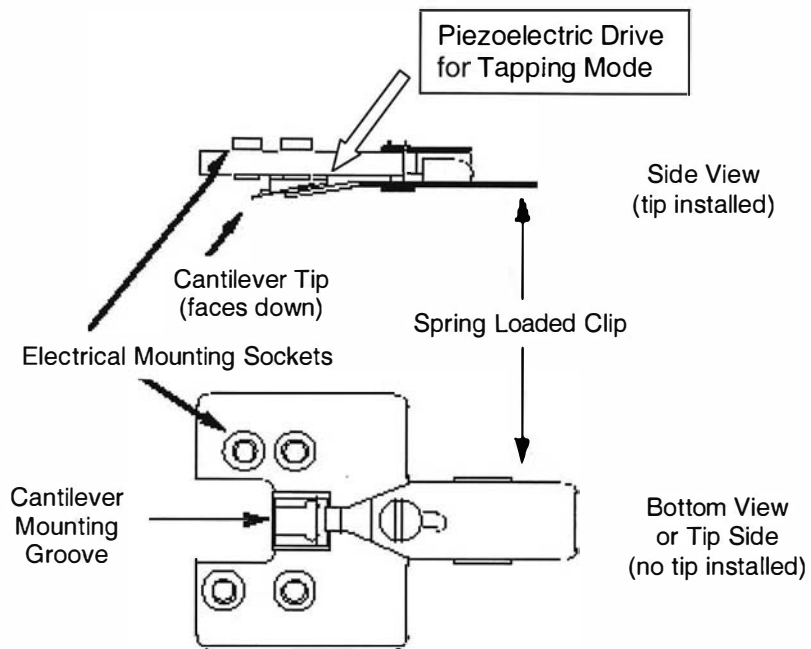
### 1.3 Chapter 1 Figures



**Fig. 1.1:** Schematic of AFM technique.

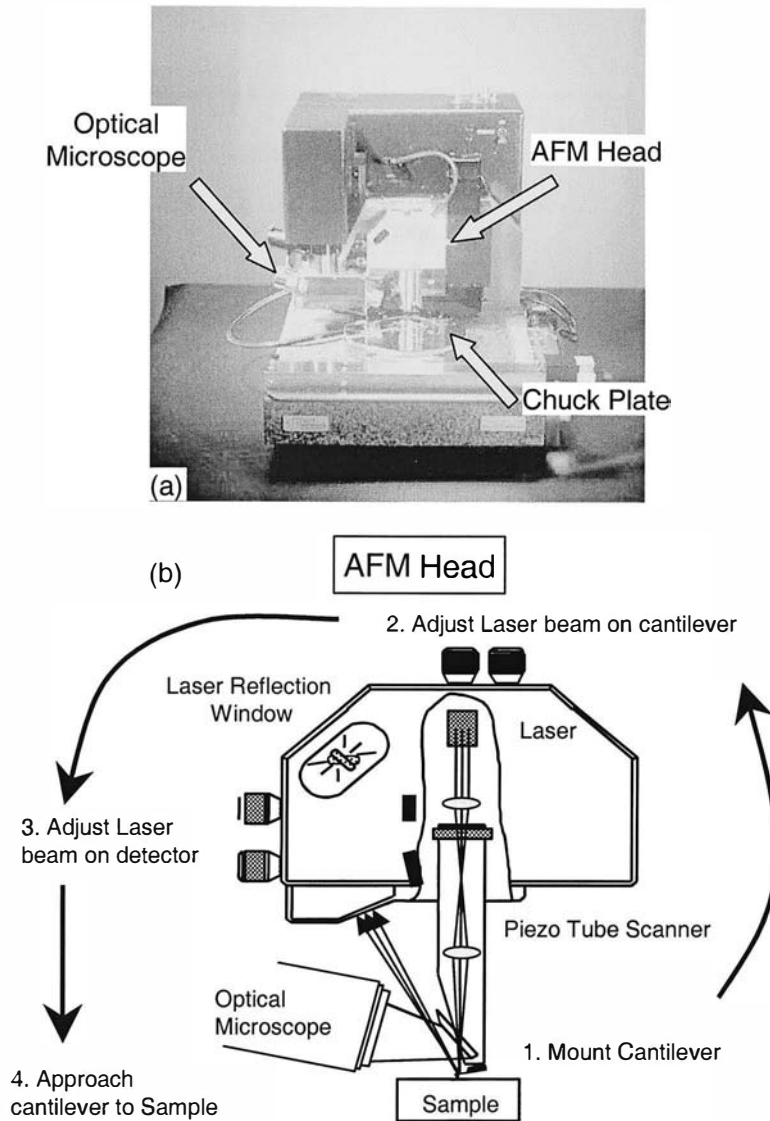


**Fig. 1.2:** (a) Si cantilever used primarily for tapping mode AFM and (b) Si<sub>3</sub>N<sub>4</sub> cantilever used for contact mode AFM.



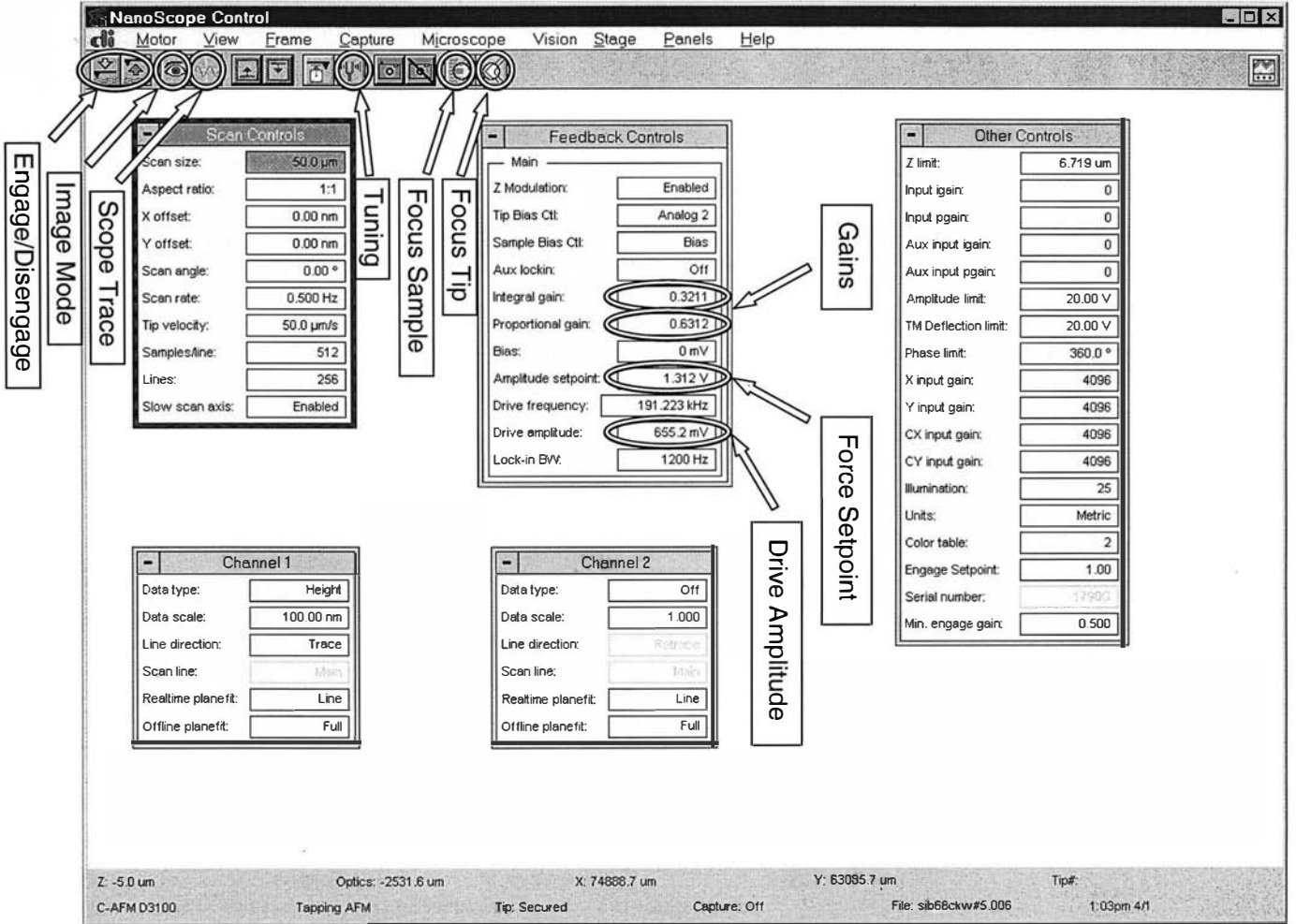
**Fig. 1.3:** Tapping mode cantilever holder.

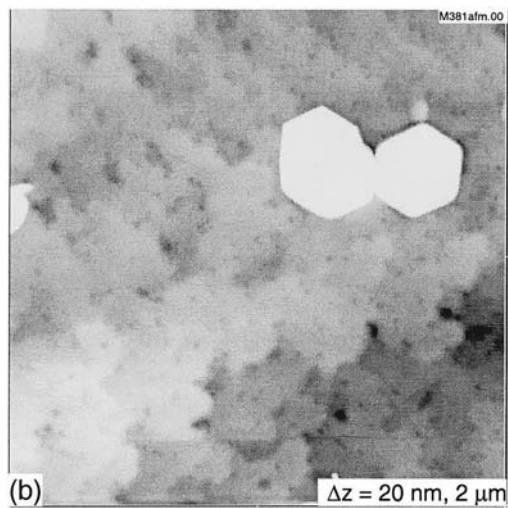
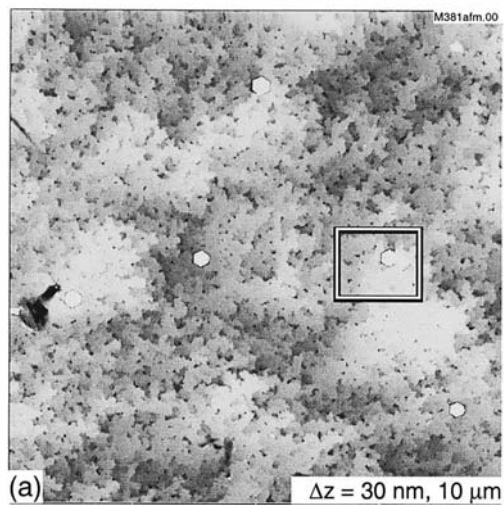




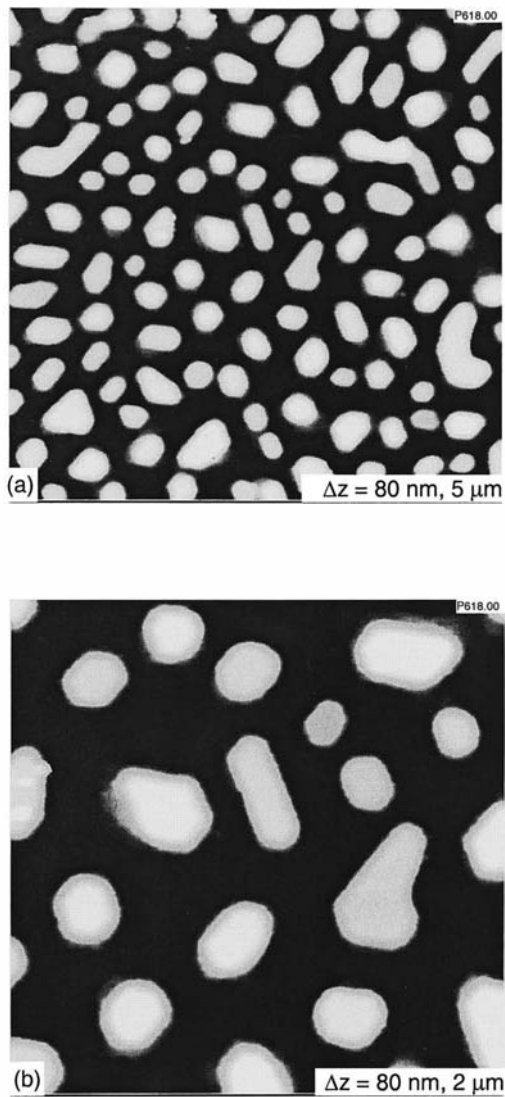
**Fig. 1.4:** (a) Dimension 3100 AFM unit and (b) schematic of AFM head.

Fig. 1.5: AFM Data Screen with important icons and data values highlighted.





**Fig. 1.6:** AFM images of Ga-polar GaN, where the z-height data range and image size are indicated in the lower right corner of each image.



**Fig. 1.7:** AFM images of N-polar GaN, which is significantly more rough than Ga-polar GaN (compare to Fig. 1.6).

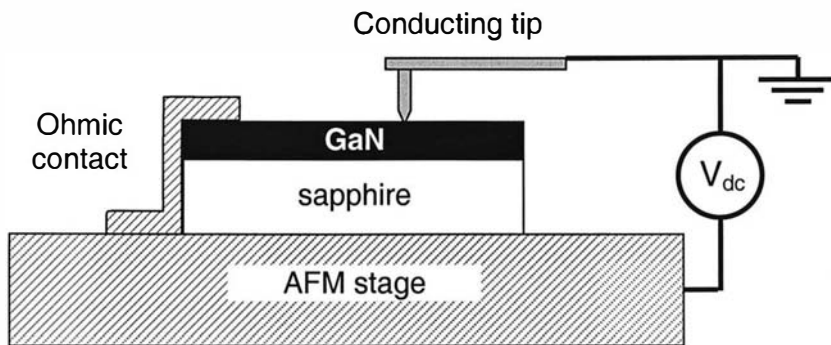


**Fig. 1.8:** Conductive AFM (CAFM) and Tunneling AFM (TUNA) techniques, where a tip-sample current is measured for an applied DC bias voltage.

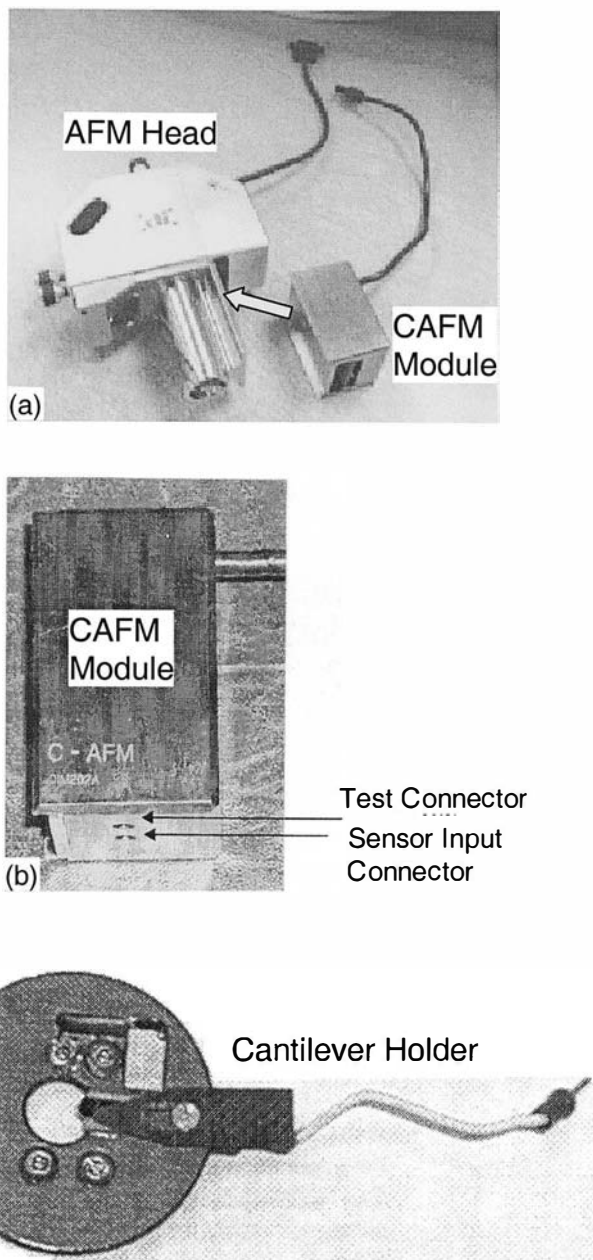


**Fig. 1.9:** (a) AFM head and CAFM module attachment, (b) close-up of module, and (c) CAFM cantilever holder with current detection.

Fig. 1.10: CAFM Data Screen with important values highlighted.

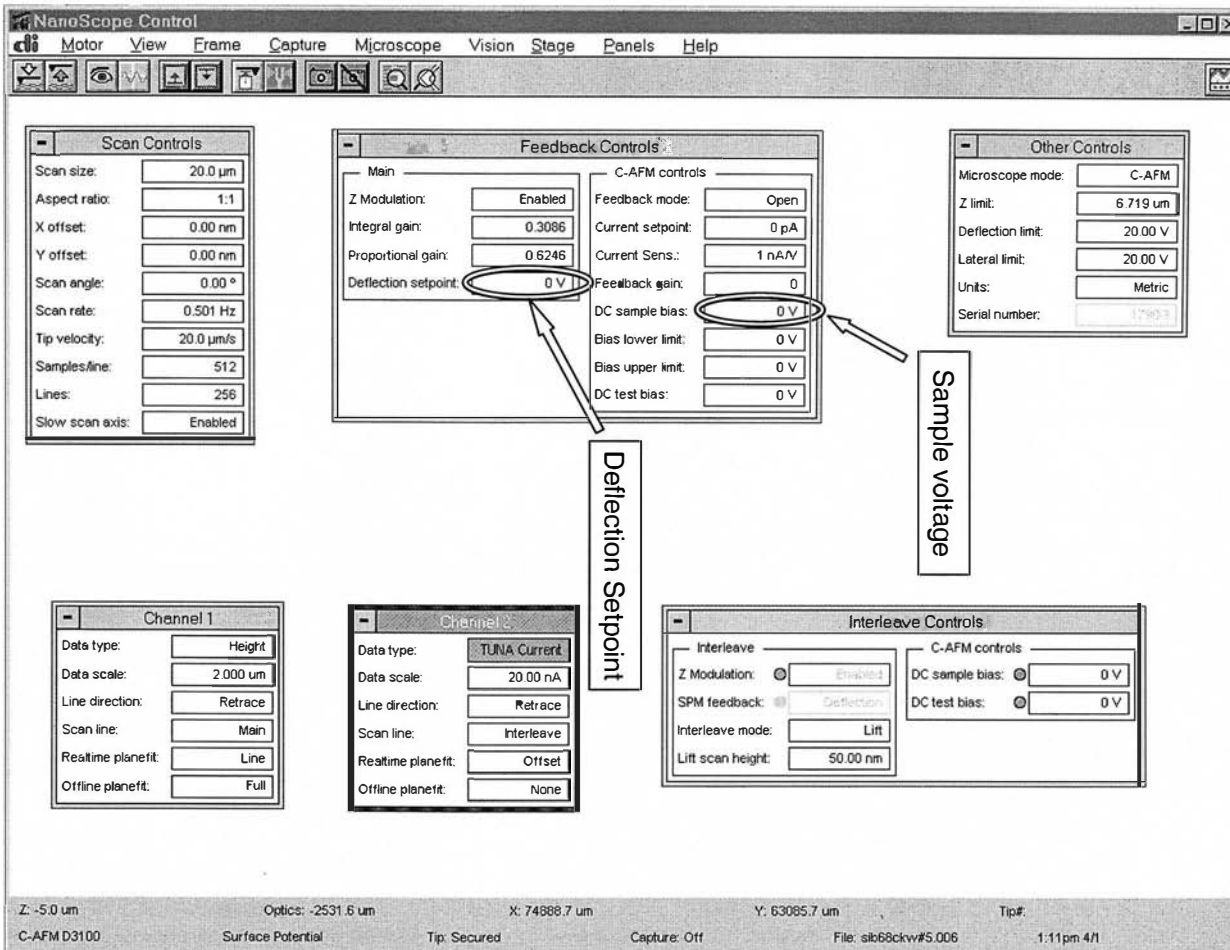
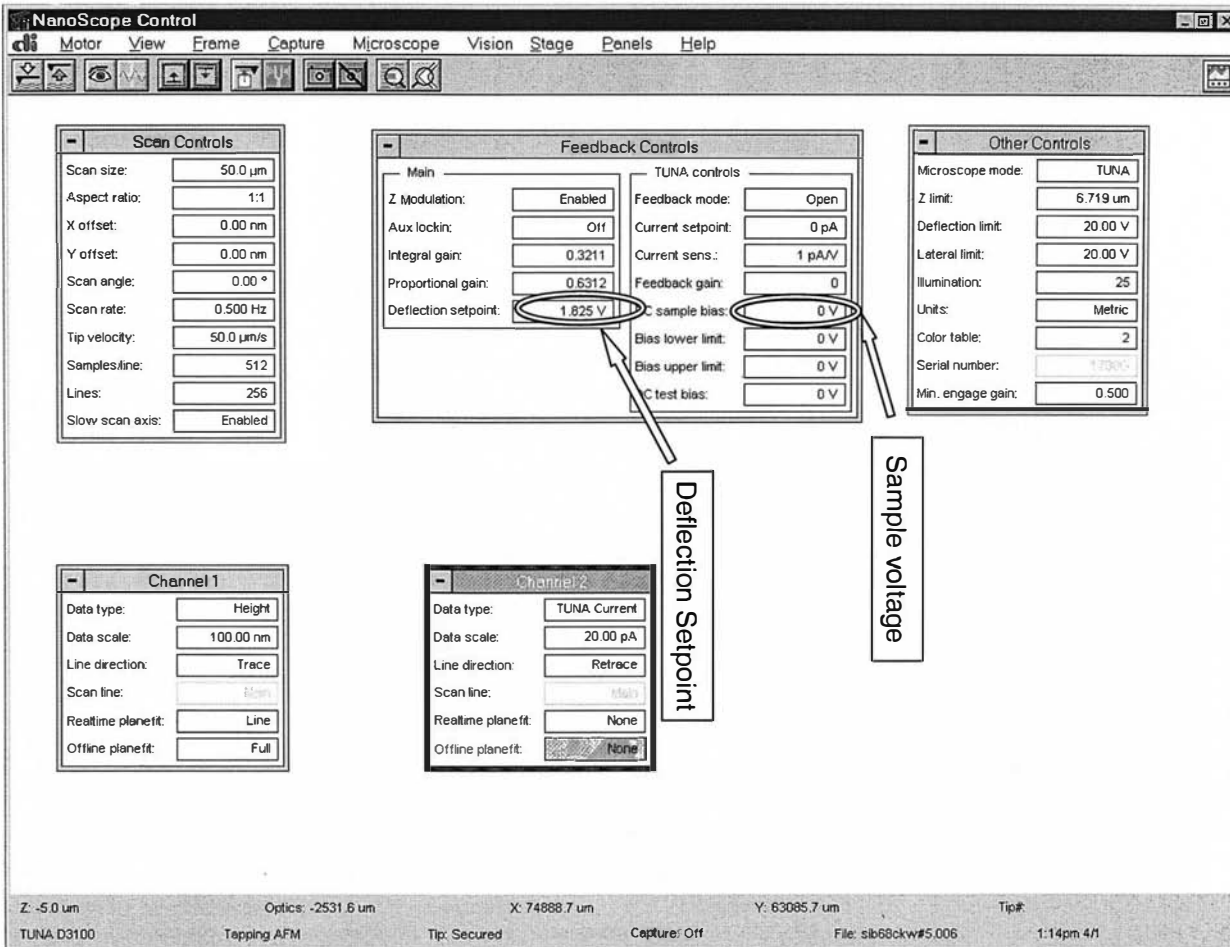
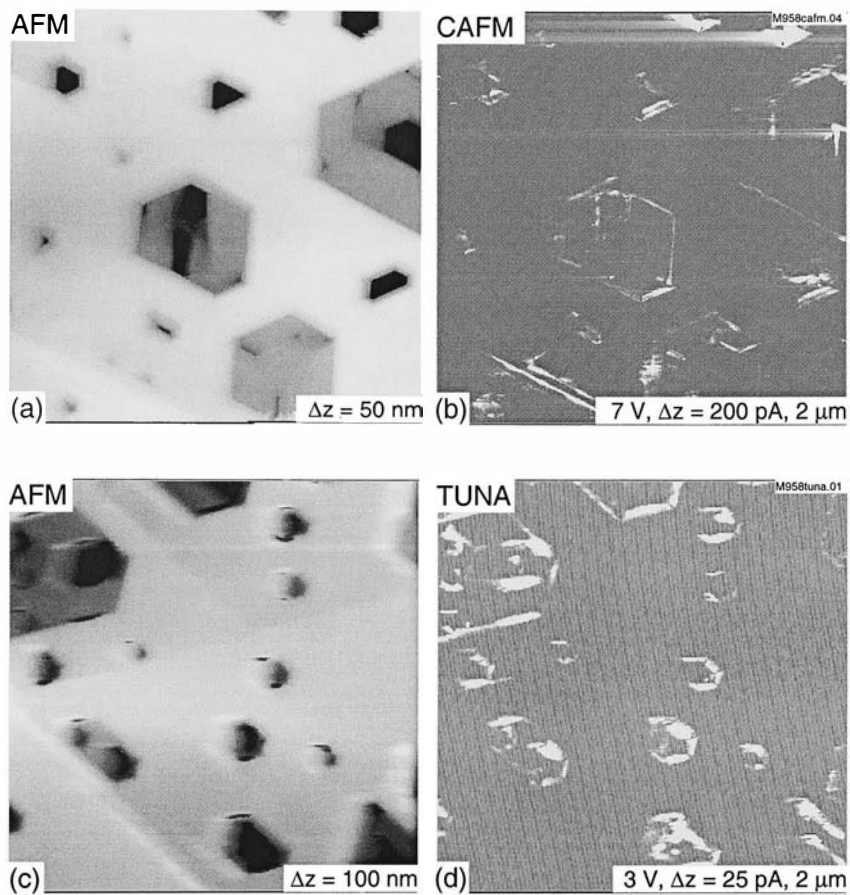


Fig. 1.11: TUNA Data Screen with important values highlighted..







**Fig. 1.12:** (a, b) AFM & CAFM and (c,d) AFM & TUNA images of etch pits on n-type GaN using positive sample bias (reverse-bias).

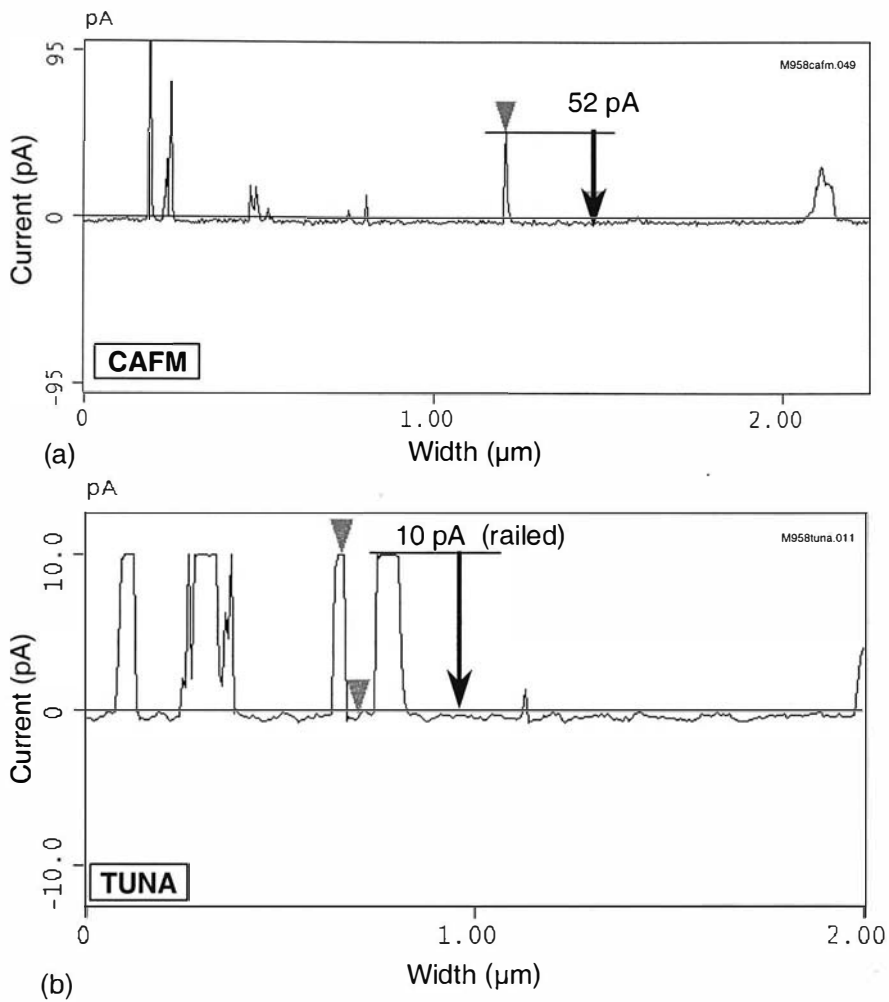


**Fig. 1.13:** Cross sections for CAFM and TUNA images shown in Fig. 1.12.

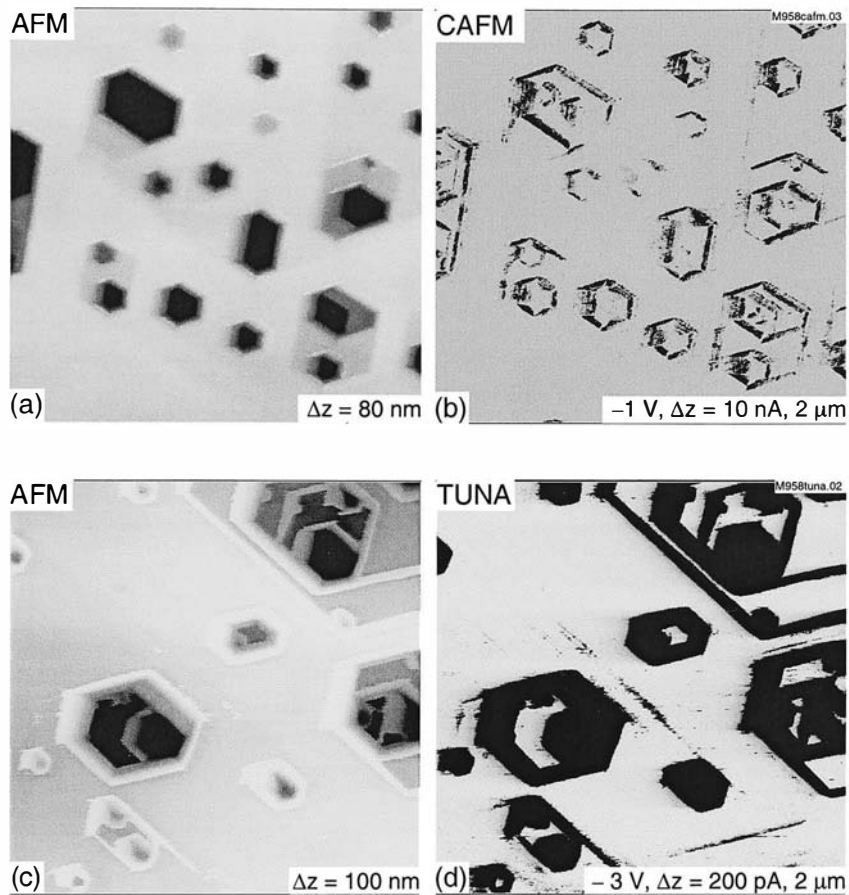


**Fig. 1.14:** (a, b) AFM & CAFM and (c,d) AFM & TUNA images of etch pits on n-type GaN with negative sample bias (forward-bias).

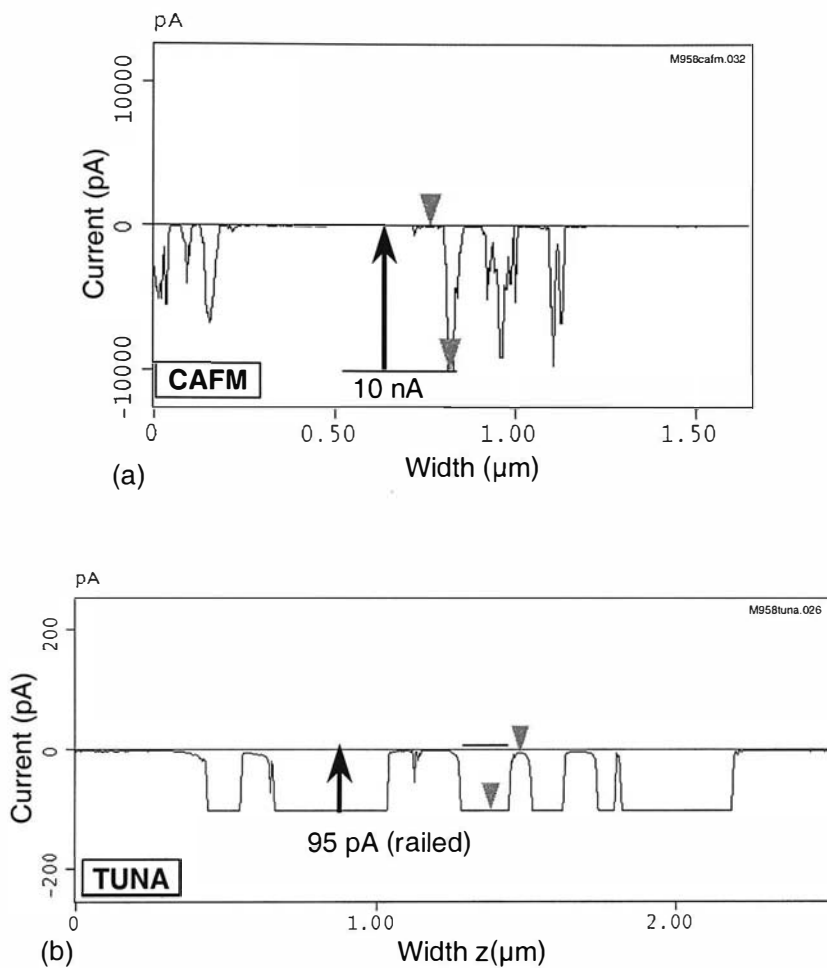


**Fig. 1.15:** Cross sections for CAFM and TUNA images shown in Fig. 1.14.

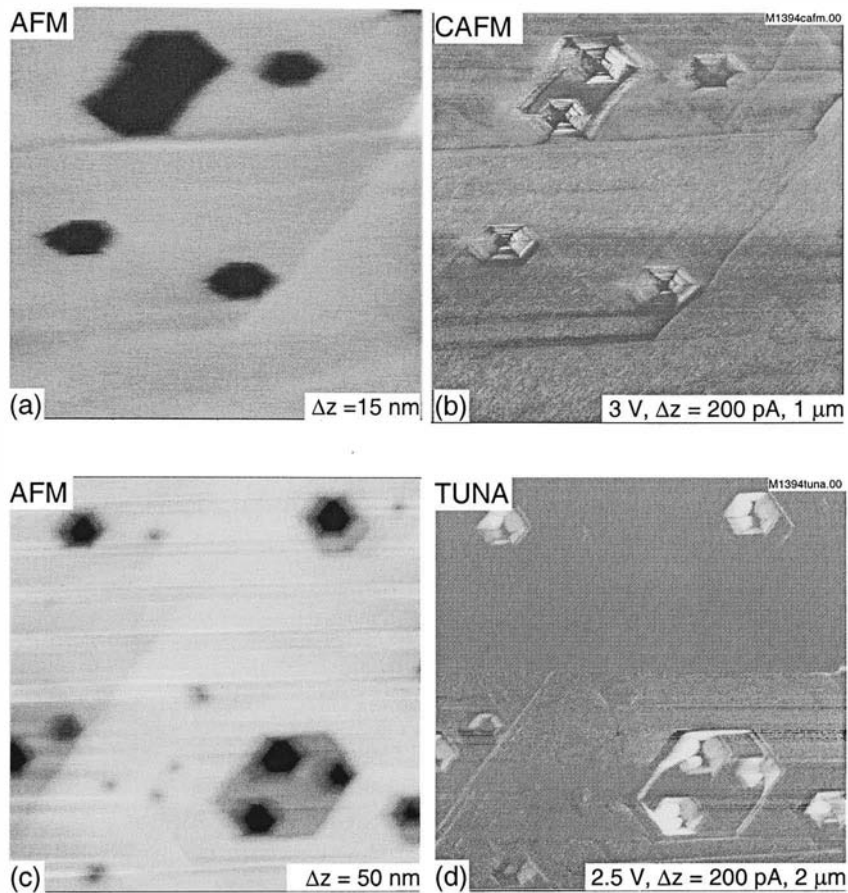


**Fig. 1.16:** (a, b) AFM & CAFM and (c,d) AFM & TUNA images of p-type GaN with positive sample bias (forward-bias).

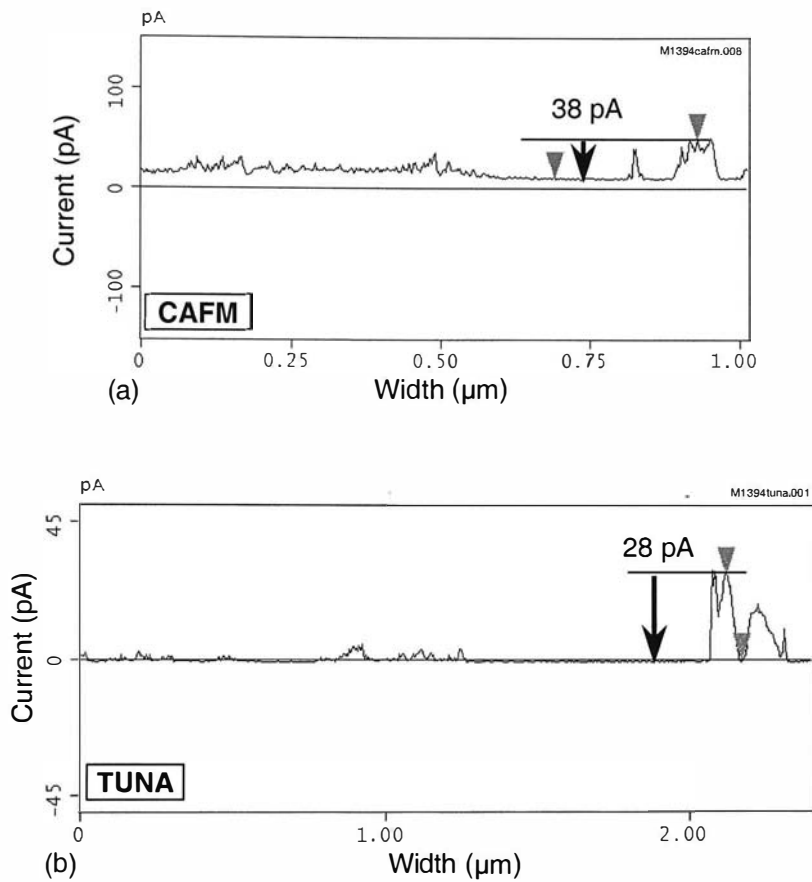


**Fig. 1.17:** Cross sections for CAFM and TUNA images shown in Fig. 1.16.

## Chapter 2. Surface Potential Electric Force Microscopy

### 2.1 Technique

Electric Force Microscopy (EFM) uses a conductive AFM cantilever to probe the electric forces between the tip and locally charged regions on a surface. In a variation of this technique known as Surface Potential EFM, a feedback loop is utilized to map out the local surface contact potential in real-time. This technique is also referred to as Kelvin probe force microscopy (KPFM) in the literature [12]. A step-by-step outline of SP-EFM is shown in Figs. 2.1 and 2.2. In addition, the data screen for taking SP-EFM data is shown in Fig. 2.3.

During the first scan while taking SP-EFM data (see Fig. 2.1a), tapping mode topography data is acquired by mechanically oscillating the cantilever at its resonance frequency and recording the tip height necessary to maintain a constant tip-sample force. This data produces the AFM topography image, which will be correlated with SP-EFM data acquired during a second scan in the same location. After the first scan is complete, the cantilever is raised to a set “Lift Height” above the sample surface and an AC voltage ( $\omega$ ) is applied to the conductive tip. This voltage results in an electric force between any locally charged regions on the surface and the tip. The increased tip-sample distance is necessary to enhance longer-range electric forces with respect to shorter-range forces such as Van der Waals forces.

During the second scan, the cantilever again begins to oscillate, but this time the oscillation is due to an electric force between the tip and sample. This force actually has a DC and two AC ( $\omega$ ,  $2\omega$ ) force components (see Fig. 2.2b), where the coefficient of the  $\omega$  force component is dependent on the difference in the DC voltage potential between the tip and sample [13]. Therefore, a feedback loop can be used to measure the local surface potential  $V_{sp}$  by changing the applied DC tip voltage such that the  $\omega$  force component becomes zero. This applied DC voltage then reflects the local surface contact potential at the tip location. This voltage data produces the SP-EFM image which is nearly simultaneously acquired with the AFM image. Features in the SP-EFM data can

then be compared to those in the AFM data, possibly leading to the identification of sources of locally induced surface potential.

## 2.2 Detection of Inversion Domains

There has been an increased interest in the use of III-nitride semiconductors primarily for their use in high power and high temperature electronic devices [14]. Unfortunately, such devices do not achieve optimal performance due to the presence of inversion domains that cause increased carrier scattering [15,16]. An inversion domain (ID) is a local region of the film having the opposite polarity (or crystal orientation) with respect to the film itself. The two possible orientations of c-axis GaN are Ga-polarity (0001) and N-polarity ( $\overline{0001}$ ), where the top layer is terminated by Ga or N atoms, respectively (see Fig. 2.4a). The technique of SP-EFM can be used to distinguish between these two polarities, where N-polar regions are lower in potential than Ga-polar ones (see Fig. 2.4b).

In Figs. 2.5 to 2.7, three different Ga-polar surfaces are examined using AFM and SP-EFM. The first two samples were grown in the Riber system (sample #1376 and #6566) and the last sample in the SVT system (#381) of the Morkoç group. In all three figures, the conditions for the SP-EFM data are noted above the cross section, where the AC driving amplitude voltage (DA) ranges from 4 to 6 V, and the lift height (LH) is typically ~50 nm. In Fig. 2.5, the AFM image shows a smooth surface with a pit in the lower left area and a small island in the upper right. The corresponding SP-EFM image indicates no change in surface potential for the pit, but a change of -90 mV for the island. This negative potential value indicates the presence of a N-polar inversion domain on the Ga-polar film. Fig. 2.6 shows a more “bumpy” surface with a number of very small pits (<100 nm dia.). In this case, the SP-EFM image shows a single dark region corresponding to an inversion domain located at a somewhat more raised island region on the surface. Unlike for the previous sample, the topography signature of the inversion domain is not obvious. It should also be noted that the potential change is only -30 mV for this particular sample. Our observed values for the difference in surface potential between the Ga and N-polar regions are roughly consistent with previous work in the



group by Jones et al. [3]. For a reference sample of Ga and N-polar films grown on sapphire, it was found that Ga-polar (or N-polar) GaN had a relative voltage difference of  $25 \pm 10$  mV (or  $-30 \pm 10$  mV) with respect to the sapphire substrate. This resulted in a surface potential of  $-55$  mV for the N-polar film with respect to the Ga-polar one.

Because different potential values have been measured for the ID's, the effect of lift height or drive amplitude should be considered. Our data show that drive amplitude does not affect the measured surface potential. In the case of lift height, however, there can be a measurable change. If the lift height is significantly decreased to below 10 nm, the coupling with topographical data is strong and influences measured values. If the lift height is significantly increased above 200 nm, we have also observed a change in the measured inversion domain surface potential, as shown in Fig. 2.7. At lift heights of 80 nm and 400 nm, the ID potential changes from  $-26$  mV to  $-40$  mV, respectively (see Fig. 2.7c-d corresponding to right-most circle in Fig. 2.7b). If the lift height is maintained between 50 and 200 nm, however, no significant change in measured surface potential has been observed. It should be noted that Fig. 2.7 shows areas of *higher* surface potential at locations of irregular islands on the surface, as indicated by the left-most circles in Fig. 2.7b. At this time, it is not clear as to what these regions of higher potential represent.

### 2.3 Application to Modulation Doped Field Effect Transistors

Due to their large energy band gaps, III-nitride semiconductors have attracted substantial interest with regard to Modulation Doped Field Effect Transistors (MODFETs). AlGaIn/GaN MODFETs grown on semi-insulating SiC are capable of 5 to 10 times the power density of AlGaAs/GaAs MODFETs [17]. A typical energy band diagram of an AlGaIn/GaN MODFET is drawn in Fig 2.8b. The carriers are confined to a two-dimensional electron gas (2DEG) in the active GaN layer due to band bending caused by spontaneous and piezoelectric polarization charges. The piezoelectric polarization in the strained AlGaIn induces electric fields that increase the sheet carrier concentration and narrow the 2DEG confinement [18]. To reduce electron scattering

from ionized impurities in the doped AlGa<sub>N</sub>, a thin spacer layer of undoped AlGa<sub>N</sub> is typically used adjacent to the active GaN layer.

Two different MODFETs were used in this study: 1) MODFET #1 with no GaN spacer layer between the active AlGa<sub>N</sub> layer and top metallization, and 2) MODFET #2 with a GaN spacer layer (see Fig. 2.8a). The MODFET's used in this study have typical gate widths of ~300 μm and lengths of ~2 to 5 μm (see optical image in Fig. 2.9a). In Fig. 2.9c-d, the SP-EFM image of MODFET #1 with no applied voltage shows that the top AlGa<sub>N</sub> layer is 13 mV higher in potential than the adjacent source/gate/drain metallization. When an external negative voltage is applied such that the gate is biased negative with respect to the grounded source, the SP-EFM data show a measured surface voltage that is significantly lower than expected, in fact only ~45% of the applied voltage (see Fig. 2.10). When a positive gate voltage is applied, the measured surface potential is again lower in magnitude than it should be (see Fig. 2.11). The discrepancy between the surface voltages measured by SP-EFM and the applied voltages has not yet been resolved. This phenomenon is not isolated to one device, however. Figures 2.12 and 2.13 show MODFET #2, which has a thin GaN spacer layer between the metallization and the Si-doped AlGa<sub>N</sub> active layer, with two different negative gate bias voltages. In both cases, the measured gate potential is ~65% of the applied voltage. The fact that these measured voltages are a higher percentage of the applied voltages as compared to MODFET #1 indicates that this discrepancy is more than instrumental error. This preliminary study has confirmed that SP-EFM can be used to image the local potential changes of MODFET's under operation, although the absolute voltage values are not as expected. Future studies will operate the MODFET at AC frequencies and use local SP-EFM measurements to monitor changes in surface potential due to charge trapping and other phenomena.

In conclusion, variations of AFM have been used to study the electrical characteristics of GaN films and devices. Conductive AFM (CAFM) and Tunneling AFM (TUNA) studies have shown that prismatic planes present on etch pits and as-grown islands show enhanced conductivity, indicating possible leakage paths in device applications. Further studies on samples grown with well-controlled prismatic planes

may help explain whether such enhanced conductivity is related to dislocations or different Schottky barrier heights. The technique of Surface Potential Electric Force Microscopy (SP-EFM) has also been used to characterize GaN films. The identification of N-polar inversion domains in Ga-polar films has been demonstrated, where potential difference values ranging from 30 to 90 mV have been measured. In addition, the local potential on MODFET devices has been imaged, indicating the viability of future studies on such devices during operation.

## 2.4 Chapter 2 Figures

### 1st Scan

Obtain topography scan in tapping mode.  
(Cantilever mechanically oscillated at resonance with piezoelectric.)

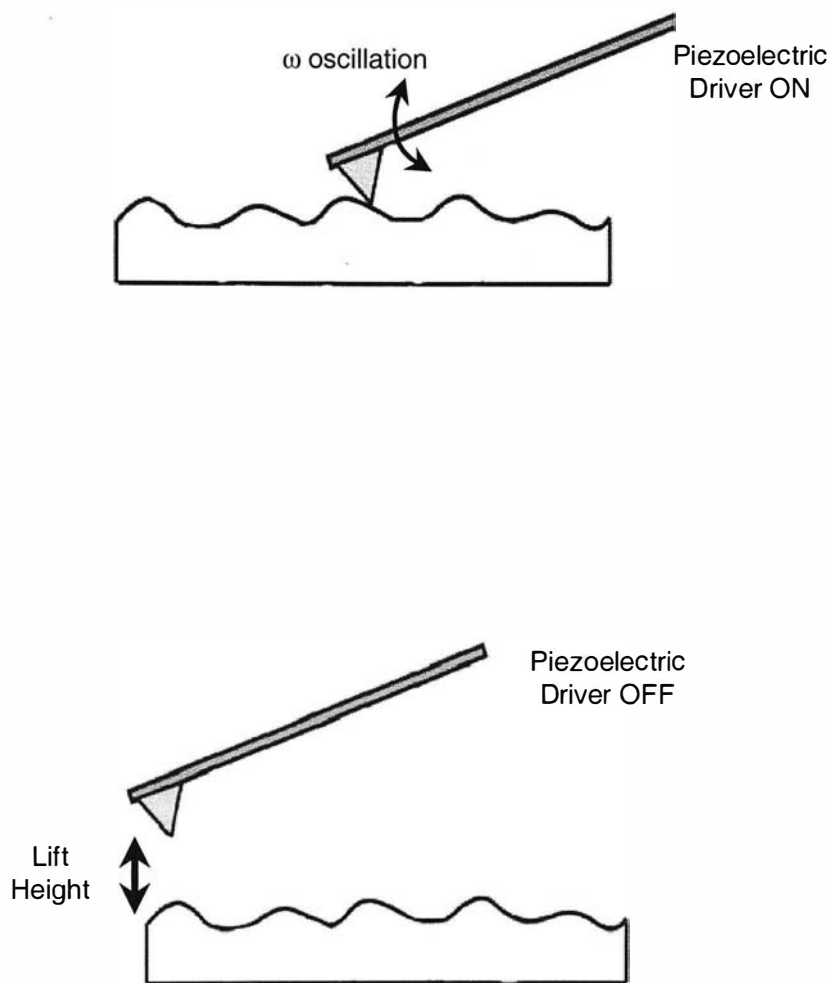


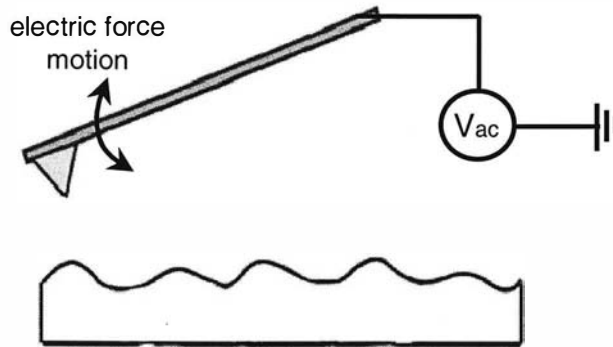
**Fig. 2.1:** Step-by-step explanation of Surface Potential Electric Force Microscopy (SP-EFM) technique.

### Setup for 2nd Scan

AC Voltage ( $\omega$ ) applied to metallized tip.

Results in tip-sample electric force with  $\omega$  component.

Motion of oscillating cantilever detected.



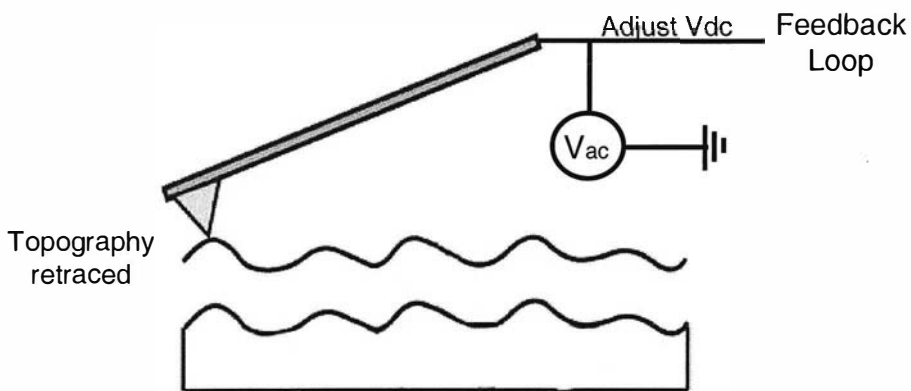
### 2nd Scan

Feedback loop adjusts DC voltage on tip to “zero”  $\omega$  force component.

Tip DC voltage then matches local surface potential  $V_{sp}$ .

SP-EFM image maps DC voltage vs. position.

Note: During scan, tip retraces topography to improve EFM signal.



$$F = -\frac{\partial U}{\partial z} = -\frac{V^2}{2} \frac{\partial C}{\partial z} \quad \text{where } V = V_{SP} + V_{DC} + V_{AC} \sin(\omega t)$$

$$F = F_0 + F_1 \sin(\omega t) + F_2 \cos(2\omega t) \quad \text{where } F_1 \propto (V_{DC} - V_{SP})$$

**Fig. 2.2:** Continuation of Fig. 2.1.

Fig. 2.3: SP-EFM Data Screen with important values highlighted.

The screenshot displays the NanoScope Control software interface with several control panels. The 'Interleave Controls' panel has two values circled in red: '4000 mV' for Drive amplitude and '50.00 nm' for Lift scan height. Arrows point from these circles to labels 'Lift Height' and 'AC voltage amplitude' respectively. The 'Other Controls' panel shows 'Microscope mode' set to 'Tapping'.

Scan Controls	
Scan size:	20.0 μm
Aspect ratio:	1:1
X offset:	0.00 nm
Y offset:	0.00 nm
Scan angle:	0.00 °
Scan rate:	0.501 Hz
Tip velocity:	20.0 μm/s
Samples/line:	512
Lines:	256
Slow scan axis:	Enabled

Feedback Controls	
Main	
Z Modulation:	Enabled
Tip Bias Ctl:	Analog 2
Sample Bias Ctl:	Bias
Aux lockin:	Off
Integral gain:	0.3086
Proportional gain:	0.6246
Bias:	0 mV
Amplitude setpoint:	1.227 V
Drive frequency:	191.223 kHz
Drive amplitude:	655.2 mV
Lock-in BW:	1200 Hz

Interleave Controls	
Interleave	
Z Modulation:	Epoke-1
SPM feedback:	Amplitude
Sample Bias Ctl:	Ground
Input feedback:	Potential
AC+DC Bias:	Tip
Aux lockin:	Off
Amplitude setpoint:	1.500 V
Drive frequency:	191.223 kHz
Drive phase:	0 °
Drive amplitude:	4000 mV
Lock-in BW:	1200 Hz
Interleave mode:	Lift
Lift scan height:	50.00 nm

Other Controls	
Microscope mode:	Tapping
Z limit:	6.719 μm
Input gain:	0.1500
Input pgain:	0.3000
Aux input gain:	0
Aux input pgain:	0
Amplitude limit:	20.00 V
TM Deflection limit:	20.00 V
Phase limit:	360.0 °
X input gain:	4096
Y input gain:	4096
CX input gain:	4096
CY input gain:	4096
Units:	Metric
Serial number:	17960

Channel 1	
Data type:	Height
Data scale:	2.000 μm
Line direction:	Retrace
Scan line:	Main
Realtime planefit:	Line
Offline planefit:	Full

Channel 2	
Data type:	Potential
Data scale:	1.000 V
Line direction:	Retrace
Scan line:	Interleave
Realtime planefit:	Offset
Offline planefit:	None

Z: -5.0 um      Optics: -2531.6 um      X: 74888.7 um      Y: 63085.7 um      Tip#:   
 C-AFM D3100      Surface Potential      Tip: Secured      Capture: Off      File: sib68ckw#5.006      1:07pm 4/1

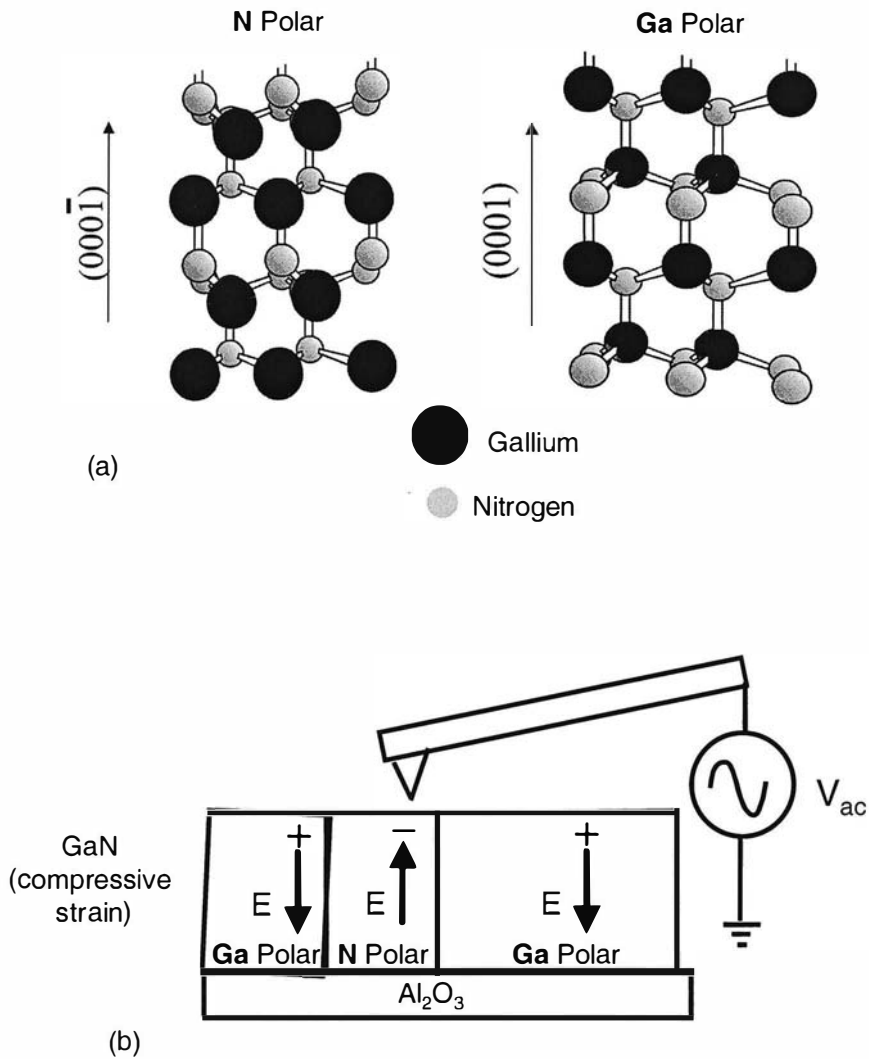


**Fig. 2.4:** (a) Crystal structures for N-polar and Ga-polar GaN and (b) schematic of local surface charging caused by domains of opposite polarity.

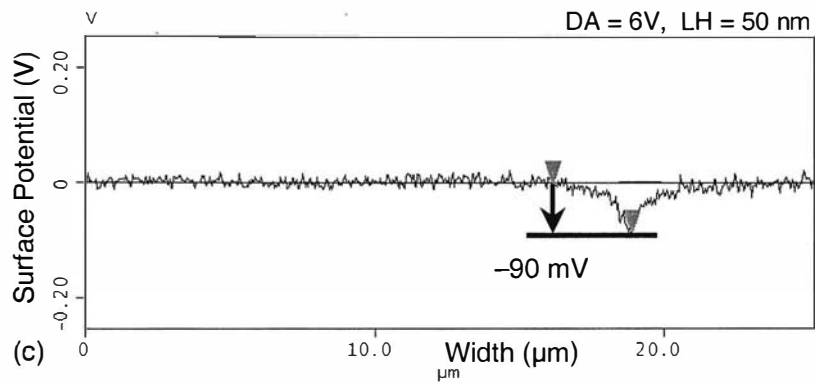
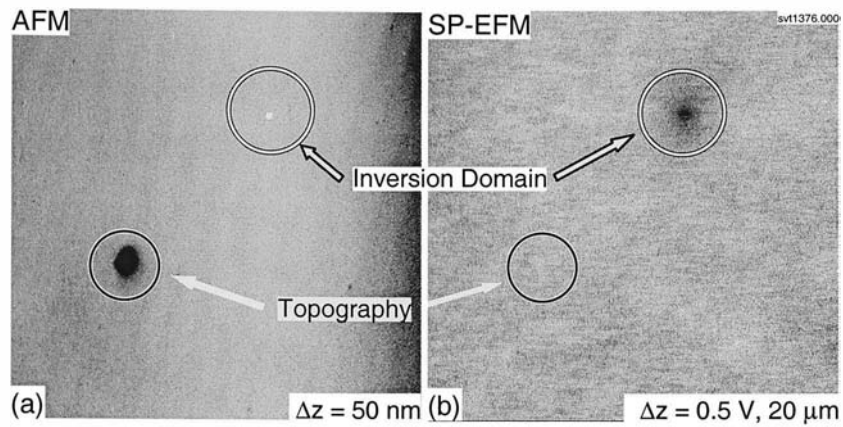


**Fig. 2.5:** (a) AFM and (b) SP-EFM images of an inversion domain on Ga-polar GaN grown with ammonia, where a cross section (c) indicates a voltage difference of 90 mV for the N-polar domain.



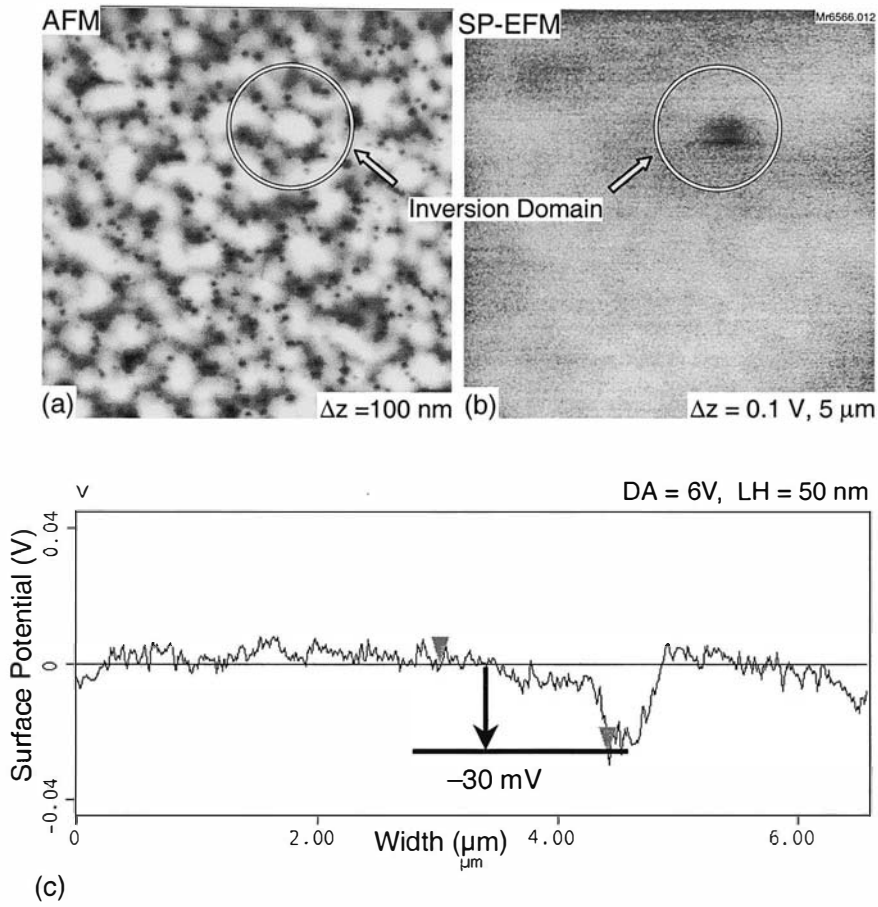


**Fig. 2.6:** (a) AFM and (b) SP-EFM images of an inversion domain on Ga-polar GaN, where a cross section (c) indicates a voltage difference of 30 mV for the N-polar domain.

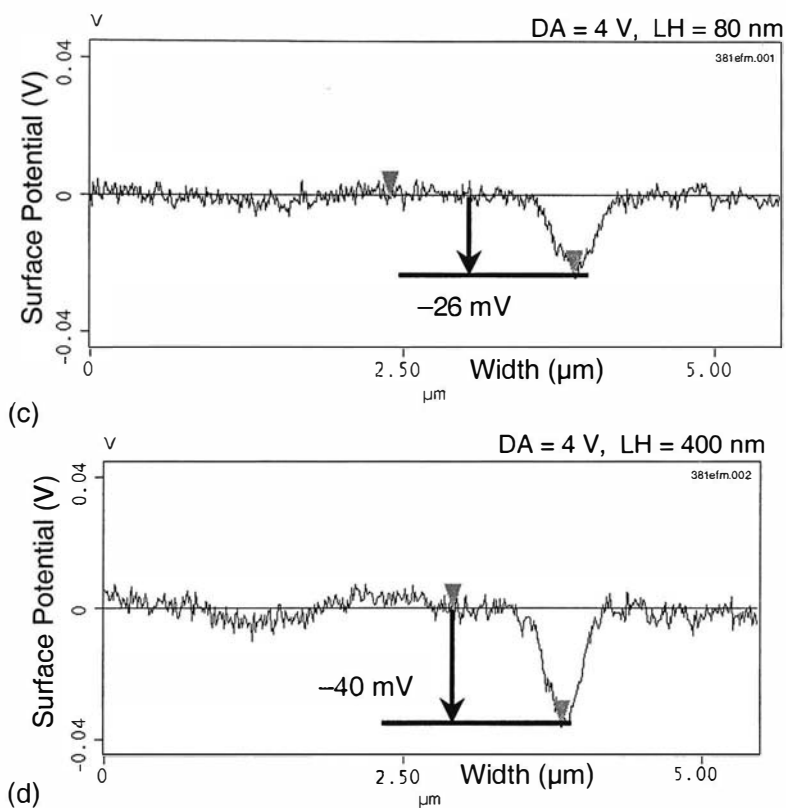
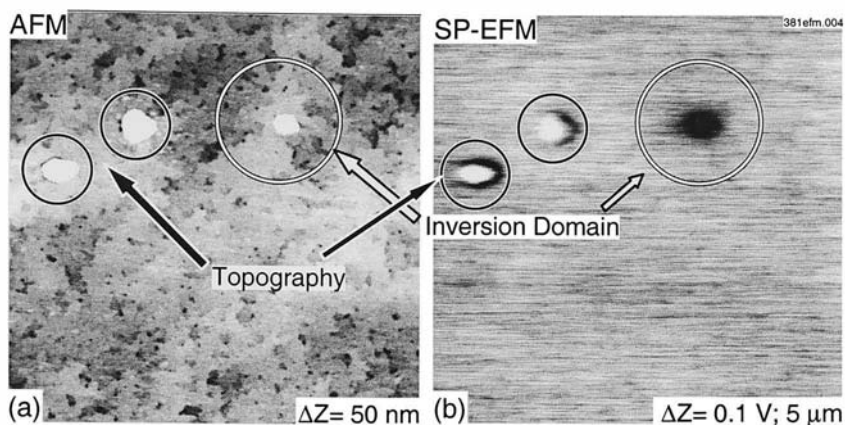


**Fig. 2.7:** (a) AFM and (b) SP-EFM images of an inversion domain on Ga-polar GaN. Cross sections of SP-EFM data are shown for lift heights of (c) 80 nm and (d) 400 nm, where larger lift heights result in a larger voltage difference for the inversion domain.

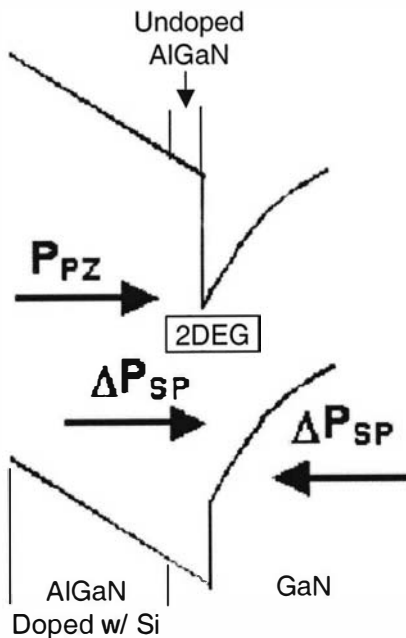
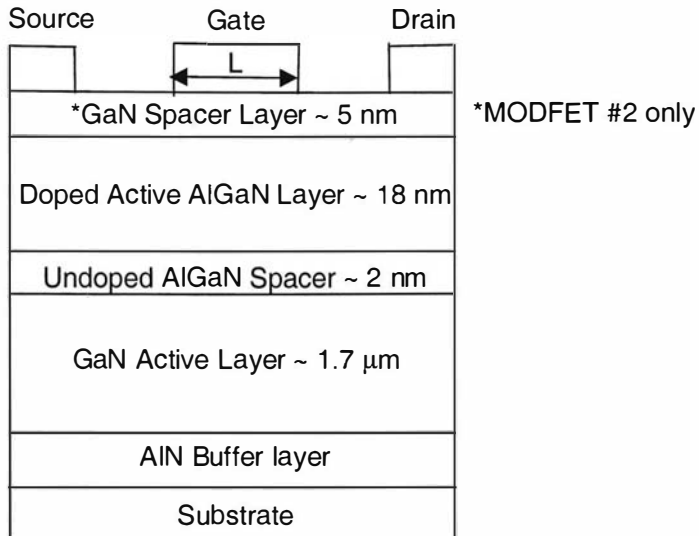


**Fig. 2.8:** (a) Schematic of a GaN/AlGaN Modulated Doped Field Effect Transistor (MODFET). (b) Band diagram showing the 2-dimensional electron gas (2DEG) that forms in the active GaN layer.

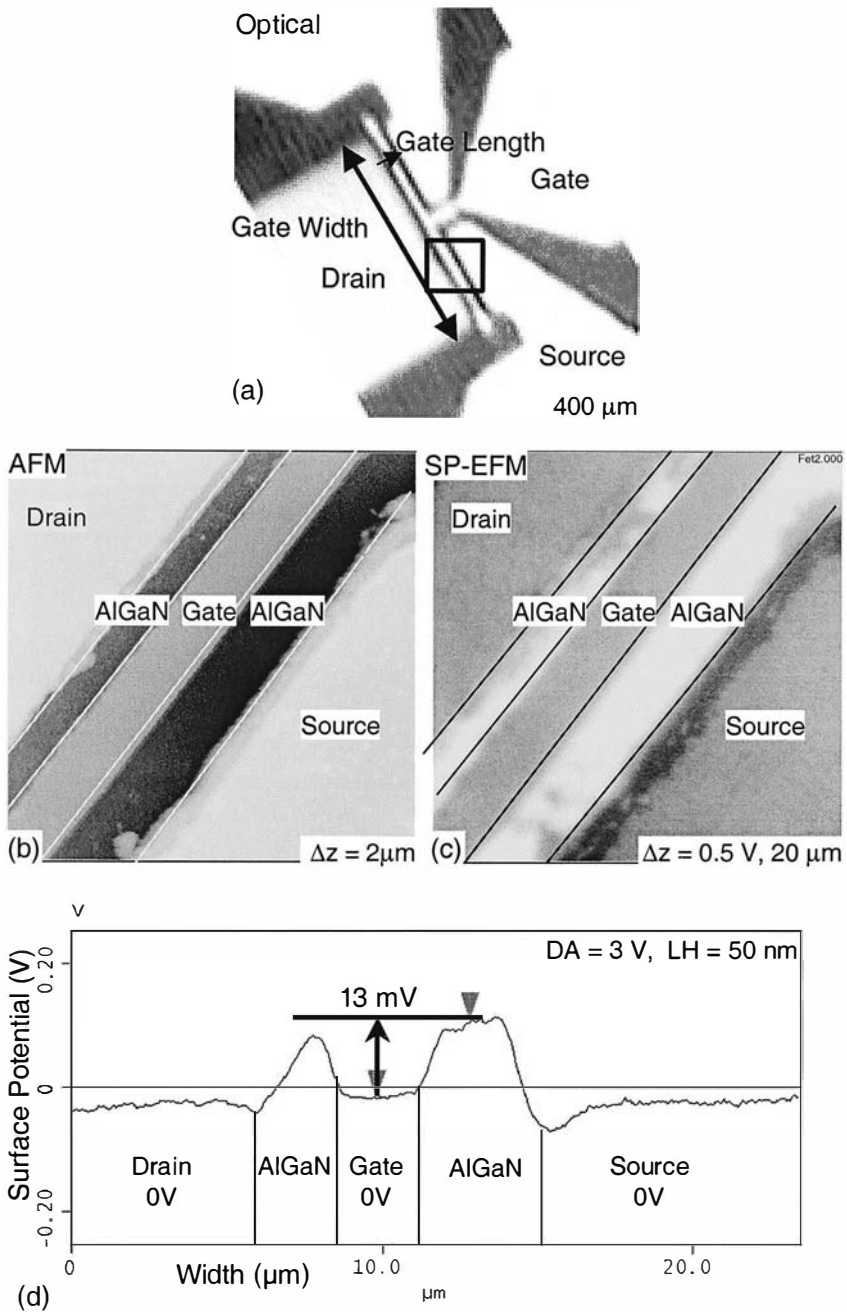


**Fig. 2.9:** (a) Optical image of MODFET #1 with an AlGaIn top layer. (b) AFM and (c) SP-EFM images taken without applied voltage. (d) Cross section of SP-EFM data indicating a 13 mV voltage difference between gate metallization and AlGaIn top layer.

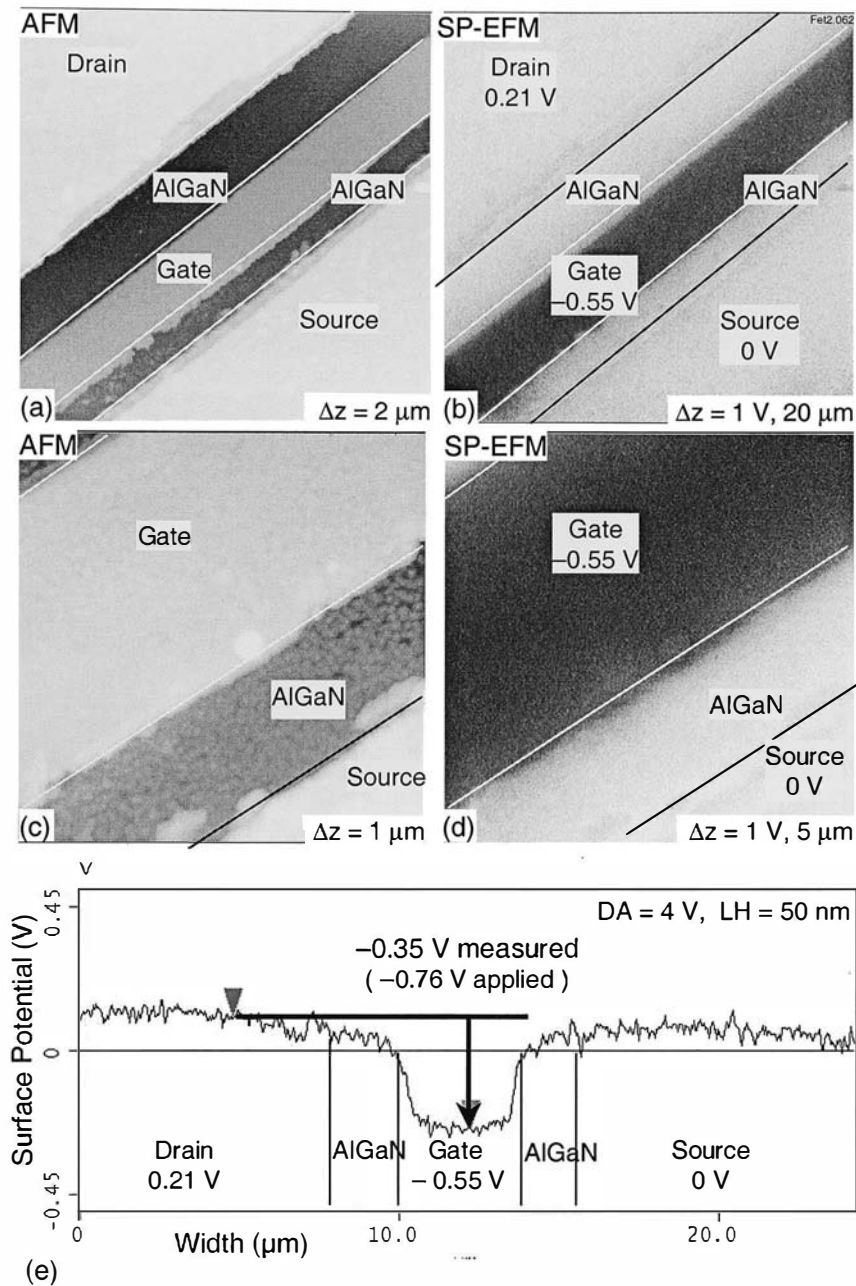


**Fig. 2.10:** (a,c) AFM and (b,d) SP-EFM images of MODFET #1 with a *negative* applied gate voltage of  $-0.55 \text{ V}$  with respect to the source.

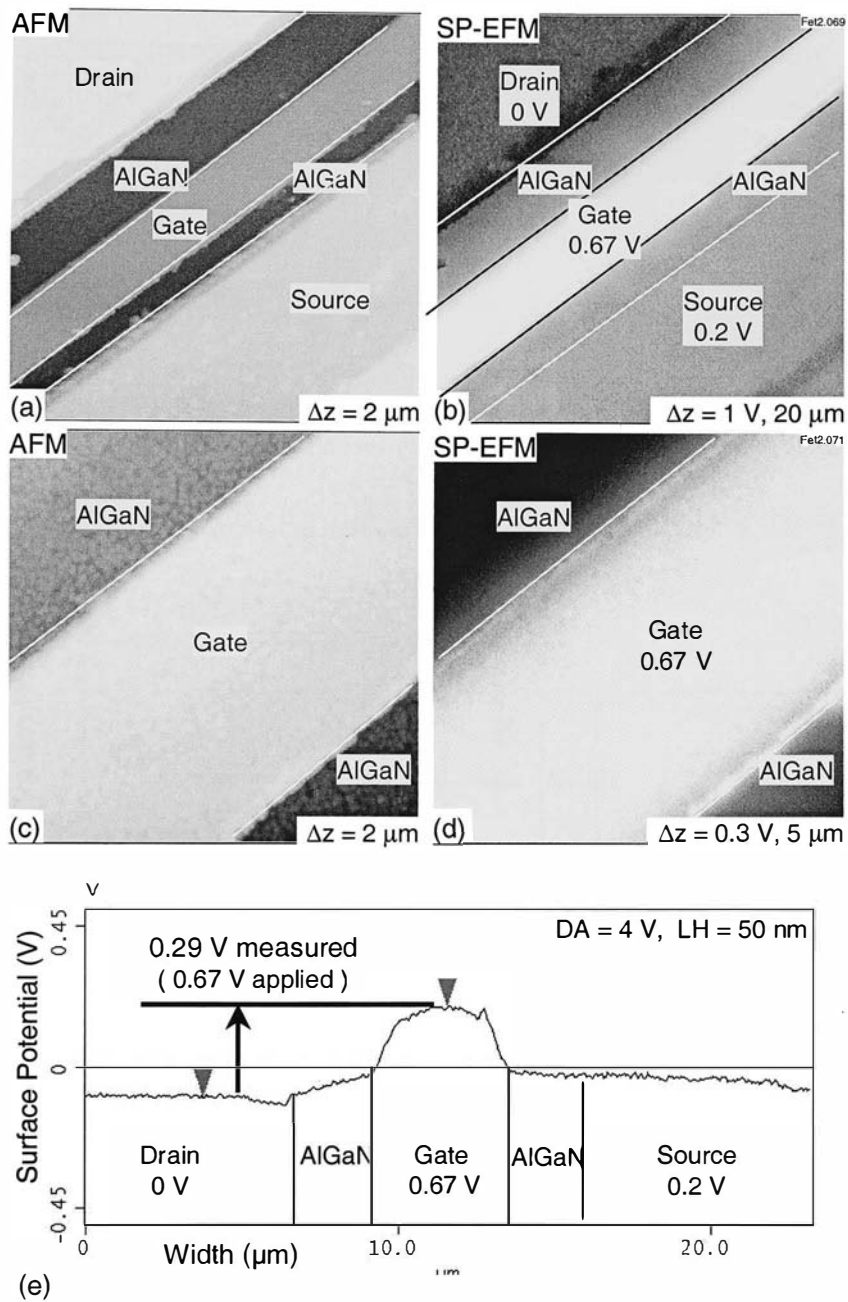


**Fig. 2.11:** (a,c) AFM and (b,d) SP-EFM images of MODFET #1 with a *positive* applied gate voltage of 0.67 V with respect to the drain.

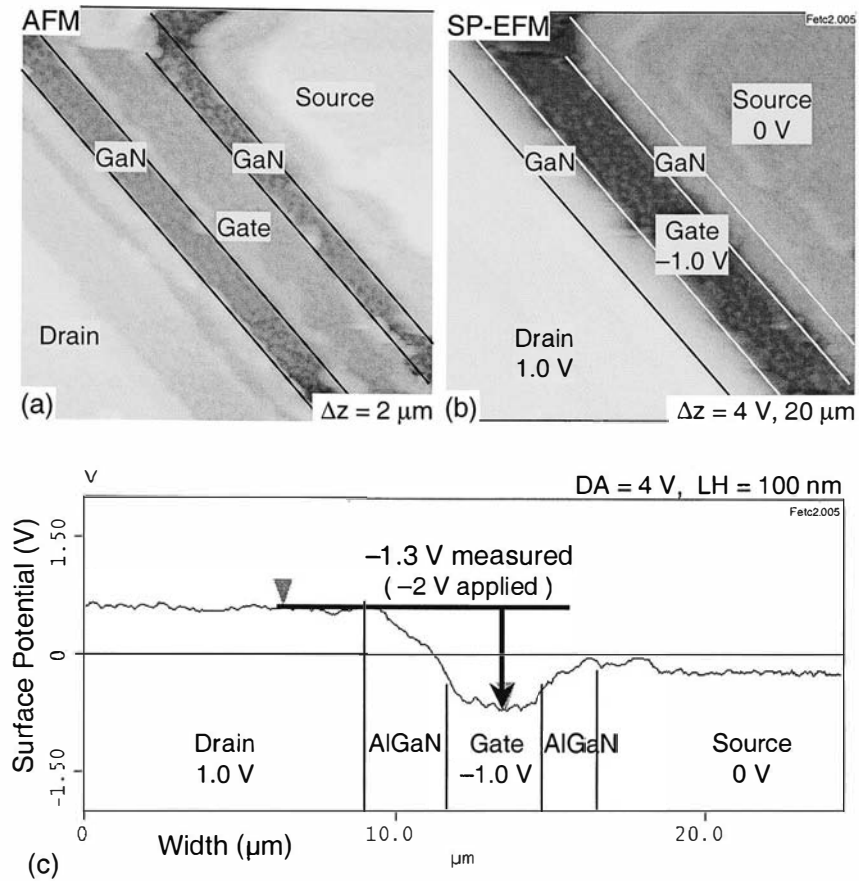


**Fig. 2.12:** (a,c) AFM and (b,d) SP-EFM images of MODFET #2 with a *negative* applied gate voltage of  $-1.0 \text{ V}$  with respect to the source.

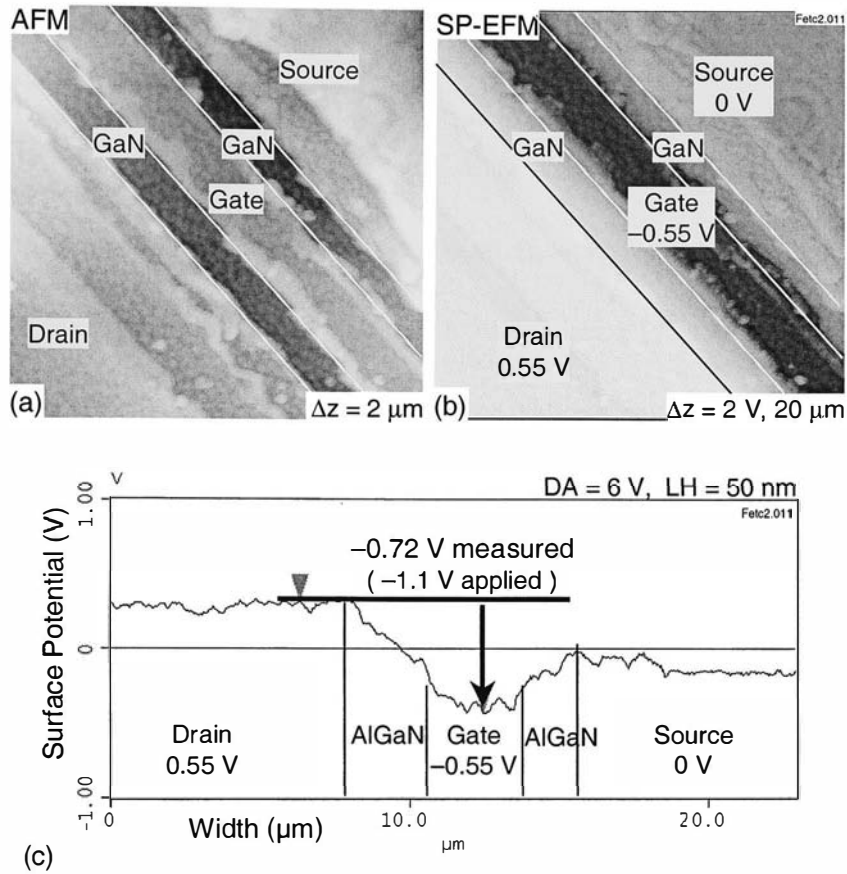


**Fig. 2.13:** (a,c) AFM and (b,d) SP-EFM images of MODFET #2 with a *negative* applied gate voltage of  $-0.55 \text{ V}$  with respect to the source.



## References

- 
- [1] Digital Instruments, Veeco Metrology Group, Dimension 3100 Manual.
  - [2] D. Huang, M.A. Reshchikov, F. Yun, T. King, A.A. Baski, H. Morkoç, Appl. Phys. Lett. **80**, 216 (2002).
  - [3] K.M. Jones, P. Visconti, F. Yun, A.A. Baski, H. Morkoç, Appl. Phys. Lett. **78**, 17 (2001).
  - [4] D. Huang, P. Visconti, K.M. Jones, M.A. Reshchikov, F. Yun, A.A. Baski, T. King, H. Morkoç, Appl. Phys. Lett. **78**, 4145 (2001).
  - [5] Digital Instruments, Conductive Atomic Force Microscopy and TUNA Manuals.
  - [6] A.A. Pomarico, D. Huang, J. Dickinson, A.A. Baski, R. Cingolani, H. Morkoç, Appl. Phys. Lett **82**, 12 (2003).
  - [7] P. Visconti, K.M. Jones, M. A. Reshchikov, R. Cingolani, H. Morkoç, Appl. Phys. Lett **77**, 3532 (2000).
  - [8] J. W. P. Hsu, M. J. Manfra, D. V. Lang, S. Richter, S. N. G. Chu, A. M. Sergent, R. N. Kleiman, L. N. Pfeiffer, and R. J. Molnar, Appl. Phys. Lett. **78**, 1685 (2001).
  - [9] J. W. P. Hsu, M. J. Manfra, S. N. G. Chu, C. H. Chen, L. N. Pfeiffer, and R. J. Molnar, Appl. Phys. Lett. **78**, 3980 (2001)
  - [10] E.J. Miller, D.M. Schaadt, E.T. Yu, C. Poblenz, C. Elsass, J.S. Speck, J. Appl. Phys. **91**, 9821 (2002).
  - [11] K. Shiojima and T. Suemitsu, J. Vac. Sci. Technol. B **21**, 698 (2003)
  - [12] M. Nonenmacher, M.P. O'Boyle, M.K. Wickramasinghe, Appl. Phys. Lett. **58**, 2921 (1991).
  - [13] J.W.P. Hsu, H.M. Ng, A.M. Sergent, Appl. Phys. Lett. **81**, 19 (2002).
  - [14] H. Morkoç, *Nitride Semiconductors and Devices* (Springer, Heidelberg, 1999).
  - [15] H. Morkoç, R. Cingolani, B. Gil, Solid-State Electron. **43**, 1909 (1999).
  - [16] H. Tang, W. Kim, A. Botchkarev, G. Popovici, F. Hamdani, H. Morkoç, Solid-State Electron. **42**, 839 (1998).
  - [17] F. Stengel, S. N. Mohammad, H. Morkoç, J. Appl. Phys. **80**, 5 (1996).
  - [18] O. Ambacher, B. Foutz, J. Smart, J.R. Shealy, N.G. Weimann, K. Chu, M. Murphy, A.J. Sierakowski, W.J. Schaff, L.F. Eastman, J. Appl. Phys. **87**, 1 (2000).